Modelling scintillation with analytic functions

Guy Potvin
DREV

Denis Dion
DREV

J. Luc Forand
DREV

Defence Research Establishment Valcartier

Technical Report

DREV TR 2001-060

2001-11-27

105-01813/

Author

Guy Potvin

Guy Potvin

Approved by

Gabriel Otis

Gabriel Otis

Section Head

Abstract

The general theory and physical principles describing scintillation for a system with arbitrary source and receiver aperture diameters, weak to moderate saturation and small inner scale, are reviewed. Analytic approximations, which describe the scintillation with an error not exceeding 35% of the exact value over a specified range of aperture diameters, inner scale and saturation, are proposed. The analytic approximations are described as the product of two functions: the first one represents the effect of nonzero source and receiver diameters in the weak saturation limit, and the other represents the effect of saturation.

Résumé

Nous avons comme objectif dans ce rapport l'établissement d'une expression analytique permettant de décrire la scintillation d'un signal détecté et généré par un système optique général, se propageant dans des conditions de turbulence allant de faible à modérée. Nous passons en revue les principes physiques de la théorie de la scintillation en fonction des diamètres de la source et du récepteur du système, ainsi que le degré de saturation et l'échelle minimum de la turbulence. L'expression analytique proposée est le produit de deux fonctions. La première fonction représente l'effet des diamètres finis de la source et du récepteur incohérents. La seconde décrit l'effet de la saturation dans le domaine étudié de diamètres et de la saturation. L'erreur entre l'expression analytique et la valeur exacte de la scintillation ne dépasse pas 35%.

This page intentionally left blank.

Executive summary

Turbulence affects both infrared and visible optical systems operating within the marine atmospheric surface layer. For instance, the image quality and the efficiency of detection algorithms depend on its strength. This report addresses the turbulence effect known as scintillation, which is the rapid fluctuation of the intensity of light after it has propagated through a turbulent medium. The scintillation of a point source as seen by a receiver with arbitrary aperture diameter has been extensively studied. Analytic expressions, easily implemented in computer models, have been developed and used in software packages such as DREV's IRBLEM. For the more general case, with arbitrary source and receiver aperture diameters, in addition to arbitrary turbulence characteristics, even a simplified theory of turbulent propagation yields an unwieldy triple integral, that can be problematic for a computer model to implement. The goal of this report, therefore, is to formulate a simple analytic expression of the scintillation for this general case, so that it can be used to improve existing marine boundary layer models.

An analytic expression for the scintillation index (the variance of the received intensity normalised with respect to the mean intensity) has been developed. It uses a correction factor that modifies the classic Rytov variance and depends on the characteristics of the optical system and the turbulence in which it operates. The Rytov variance represents the scintillation of a point source, seen by a point receiver through weak turbulence. It is found that the correction factor can be expressed as a product of two functions. The first one represents the effect of the averaging over the source and receiver apertures, while the other represents the effect of saturation. The analytic expression provides a good approximation for the exact computed values over a wide range, with a maximum error of 35% for certain extreme values of source and receiver apertures.

Potvin, G., Denis, D., Forand, J. L. 2001. Modelling the scintillation index with analytic functions. DREV TR 2001-060. Defence Research Establishment Valcartier.

P516631.PDF [Page: 8 of 62]

Sommaire

L'intérêt pour la turbulence est d'une importance croissante dans l'étude du comportement des systèmes optiques et infrarouges fonctionnant dans la couche de surface atmosphérique maritime. Par exemple, la qualité des images et l'efficacité des algorithmes de détection dépendent de l'intensité de la turbulence. Ce rapport traite de la scintillation, c'est-à-dire la fluctuation rapide de l'intensité d'une onde se propageant dans l'air en turbulence. Plusieurs études ont déjà abordé les effets causés par la turbulence sur un signal provenant d'une source ponctuelle et reçu par un système optique de diamètre arbitraire. Ces études ont permis la formulation d'expressions analytiques facilement utilisables dans un ordinateur et amélioré les résultats de certains logiciels, comme IRBLEM. En général, cependant, la formulation utilise une intégrale multiple qui dépend du diamètre de la source, du diamètre du récepteur et des caractéristiques de la turbulence. Nous proposons des expressions analytiques simples permettant d'obtenir des résultats identiques à l'intégrale sans avoir à l'évaluer. Nous espérons que ces expressions permettront d'améliorer les modèles numériques de propagation dans la couche de surface maritime.

L'indice de scintillation (la variance de l'intensité reçue normalisée par rapport à l'intensité moyenne) s'exprime par un facteur de correction modifiant la variance de Rytov classique et variant en fonction des caractéristiques du système optique et de la turbulence. La variance de Rytov représente le niveau de scintillation subi par un signal provenant d'une source ponctuelle, se propageant dans la turbulence faible et détecté par un récepteur ponctuel. Le facteur de correction peut s'exprimer comme le produit de deux fonctions. La première fonction représente l'effet des diamètres finis de la source et du récepteur. La seconde décrit l'effet de la saturation. L'erreur causée par l'expression analytique est généralement faible à l'intérieur du domaine étudié, atteignant un maximum de 35% pour des diamètres extrêmes de la source et du récepteur.

Potvin, G., Denis, D., Forand, J. L. 2001. Modelling the scintillation index with analytic functions. DREV TR 2001-060. Defence Research Establishment Valcartier.

Table of contents

Abstract i

Executive summary iii

Sommaire iv

Table of contents v

List of figures vii

Acknowledgements ix

1. Introduction 1

2. Physical overview 3
   - 2.1 Turbulence 3
   - 2.2 The classical theory 6
   - 2.3 A systems approach 10

3. General integral 14
   - 3.1 Weak scattering limit 14
   - 3.2 Intermediate regime 18
   - 3.3 Aperture averaging 19
   - 3.4 General properties 26

4. Correction factor derivation 29
   - 4.1 Weak scattering limit 29
   - 4.2 Intermediate regime 32

5. Summary and discussion 36

6. Conclusions 38

7. References 39

Bibliography 42

Distribution list.....44

List of figures

Figure 1. A schematic illustration of a point source (S) emitting spherical waves through atmospheric turbulence to a point receiver (R). The source is a distance L from the receiver and the waves have a nominal wavelength λ. As the wavefronts propagate through the turbulence, they become progressively more distorted. 5

Figure 2. The solid line is Tofsted's analytic expression for the normalised intensity variance, σ_I^2, as a function of Rytov's variance, σ_R^2. The dashed line is what we expect from the weak scattering theory. The vertical dotted line represents the threshold beyond which the weak scattering theory no longer holds. The horizontal dotted line is the asymptotic value of the normalised intensity variance in the limit of very strong scattering (saturation). 8

Figure 3. A schematic illustration of the generalised Huygens-Fresnel principle used in the systems approach. The source (disk S) is modelled as a collection of point sources forming a surface on the plane $z = 0$. Each point source, labelled $(x', y', 0)$, emits a spherical wave that propagates through the turbulence and reaches the receiver. The receiver (disk R) is modelled as a collection of point receivers, labelled (x, y, L), forming a surface on the plane $z = L$. 11

Figure 4. A schematic illustration of the scattering process behind Eq. (21). The path between the source and the receiver is divided into many independent turbulent slabs of thickness equal to the outer scale of the turbulence L_0. Each slab interacts with the incident wave (fat arrow labelled E_0) to produce a first-order perturbation E_1. The scintillation at the receiver is produced by the sum of all the perturbations. It is assumed that each slab does not interact with the first-order perturbations from previous slabs. 14

Figure 5. The path weighting function as a function of the normalised range, r. This function indicates the sensitivity of the scintillation to the turbulence located at r 16

Figure 6. The integrand of the second integral in Eq. (24). Note the main lobe with a maximum at about $y \approx 0.5$, followed by a series of much smaller lobes. 17

Figure 7. The circular overlap function given by Eq. (36), normalised with respect to the area of the circle $A = (\pi/4)D^2$ and plotted with respect to its normalised argument. 21

Figure 8. The log-amplitude covariance function for spherical wave propagation through Kolmogorov turbulence according to Fried [27] with respect to the separation distance normalised by the Fresnel zone, q/μ 22

Figure 9. A plot of the scintillation index using the exponential formula (Eq. (34) and Eq. (37)) as a function of the scintillation index evaluated using the linear approximation (Eq.

(38)). Apart from the diagonal, there is also the point-receiver case ($D=0$) as well as the cases of finite aperture ($D=0.5\mu$, $D=\mu$ and $D=1.5\mu$).....23

Figure 10. A plot of the aperture averaging function $B(x)$ described by Eq. (41). 24

Figure 11. The solid line is the exact formula for the correction factor for a point source, zero inner scale and no saturation. The boxes are the approximation given by Eq. (47), and the small black circles are Churnside's formula [12, 26].....29

Figure 12. A contour plot of the logarithm of the exact correction factor as a function of the source and receiver diameters. 30

Figure 13. A contour plot of the difference, in dB, between the approximation given by Eq. (47) and (48), and the exact correction factor. 31

Figure 14. The solid line is the exact evaluation of the integral function in Eq. (29). The circles represent the approximation given by Eq. (49). 32

Figure 15. A contour plot of the effect of saturation with respect to no saturation in percent, $100(G-1)$, estimated by numerical integration for the case where $\sigma_R^2=1$. 33

Figure 16. Two cross-sections of the saturation effect function G for the case $\sigma_R^2=1$. The solid line with the circles is the cross-section along one of the axis of the contour plot in Fig. 15, that is $\alpha=\alpha_s$ and $\alpha_r=0$, or vice-versa. The line with the squares is the cross-section along the diagonal, $\alpha_s=\alpha_r=0.5\alpha$. The dotted line is the analytic formula. 34

Acknowledgements

The authors would like to gratefully acknowledge P. Lahaie of Aerex Avionique Inc. for his help in the writing of this report. Thanks are also due to L. Bissonnette and G. Roy of DREV for their thoughtful reviews of this work.

1. Introduction

Infrared and visible optical systems operating in the marine atmospheric surface layer are affected by turbulence. Image quality, error rates in optical data transmission, and detection algorithm efficiency, all depend on turbulence. One of the effects of turbulence is scintillation: namely the rapid fluctuation of intensity of light after it has propagated through a turbulent medium. Some numerical propagation models of the marine boundary layer, such as DREV's integrated software package IRBLEM [1], can give the scintillation as seen from a receiver with an arbitrary aperture diameter, but only from a point source. A more general model is needed to describe scintillation from a source of arbitrary size.

However, estimating the scintillation of a beam propagating through turbulence with arbitrary receiver and transmitter diameters is a difficult problem. Even assuming an incoherent transmitter and weak turbulence, we are still left with a double integral, which can be time consuming to evaluate. Including the effects of saturation poses an additional problem. Aside from the fact that no satisfactory physical theory of saturation exists, and that we must use an empirically based approximation, implementing the approximation demands we turn our double integral into a triple integral. Clearly, modelling scintillation from an incoherent source with arbitrary system and turbulence parameters in a practical manner requires that we find analytic approximations. These approximations should preferably exploit previous analytic expressions for more restricted cases.

It is the goal of this work, therefore, to find a simple analytical expression for the correction factor (which is a normalised expression of the scintillation) with arbitrary system and turbulence parameters. We begin by giving a brief physical overview of the problem. This includes the major features of optical atmospheric turbulence, the classic theory of turbulent wave propagation and its extension to arbitrary optical systems. We then introduce the general integral to be used as the basis of this work. The general integral is analysed and its characteristic scales are discussed. Numerical investigations of the general integral are then performed and assessed. Finally, analytic expressions are formulated which adequately describe scintillation under fairly general circumstances while still retaining a basic simplicity.

This work was carried out at DREV between June 2000 and April 2001 under work unit 1AB11, Propagation Effects in the Marine Boundary Layer.

2. Physical overview

2.1 Turbulence

Probably the most famous, and most widely used theory of turbulence is Kolmogorov's 1941 theory of inertial range turbulence [2] (commonly referred to in the literature as K41). Kolmogorov considered turbulence with statistical properties that are uniform over time (*stationary*), space (*homogeneous*), and in all directions (*isotropic*). The *structure function* for the velocity field of this type of turbulence takes the form;

$$\left\langle \left[\; \bar{v}\left(\bar{x}+\bar{l},t\right)-\bar{v}\left(\bar{x},t\right) \; \right]^2 \right\rangle = D_v^2\left(\; l \; \right) \tag{1}$$

where the angle brackets denote a statistical average (also called an *ensemble* average). The stationarity means that the structure function is independent of time, and the homogeneity and isotropy imply that it depends only on the distance l separating the points $\bar{x}+\bar{l}$ and $\bar{x}$.

Kolmogorov further assumed that the turbulence is sufficiently active that the inertial forces (the fluid pushing against itself) are much greater than the viscous forces. This means that the velocity structure function, $D_v^2\left(\mathrm{m}^2/\mathrm{s}^2\right)$, can only depend on the separation length, $l\left(\mathrm{m}\right)$, and on the energy dissipation rate per unit mass, $\varepsilon\left(\mathrm{m}^2/\mathrm{s}^3\right)$. By dimensional arguments, we obtain the relationship,

$$D_v^2\left(l\right) = C\varepsilon^{2/3}l^{2/3} \tag{2}$$

where C is the dimensionless Kolmogorov constant with a value estimated between 0.5 and 0.6 [3]. Equation (2) is sometimes called the two-thirds law, owing to the exponent of l. Also, the Kolmogorov constant and the energy dissipation are often combined into a velocity structure constant, $C_v^2 = C\varepsilon^{2/3}$, which is used as a measure of the total turbulent energy. See Frisch [4] for a modern perspective on K41.

However, the velocity field by itself has no direct effect on the propagation of electromagnetic waves. Therefore Eq. (2) is not very pertinent. Of greater relevance is the effect of the

turbulent velocity field on the refractive index field, $n(\bar{x},t)$. It has been demonstrated [5] that the structure function for n in K41-type turbulence obeys the two-thirds law,

$$D_n^2(l) = C_n^2 l^{2/3} \tag{3}$$

where C_n^2 is the refractive index structure parameter and is a measure of the strength of the turbulent fluctuations of the refractive index. This parameter can vary anywhere from about 10^{-17} $m^{-2/3}$ for very weak atmospheric turbulence, to about 10^{-13} $m^{-2/3}$ for very strong turbulence, usually near the ground [6].

It must be emphasised that real turbulence does not conform to the two-thirds law over the entire range of separation distances. In fact, it no longer applies for distances equal to or larger than the outer scale, L_0, which represents the scale where turbulence is actually generated (the size of a turbine, for example). For atmospheric turbulence, L_0 is typically about 100 m or 0.2 times the measurement height above the ground, whichever is less [6]. However, according to Tofsted [7], the outer scale should also depend on the stability of the surface layer. Similarly, the two-thirds law fails for distances shorter than the inner, or dissipation, scale, $l_0 \propto \left(\nu^3/\varepsilon\right)^{1/4}$, where ν is the kinematic viscosity of the air. At this scale, viscous forces become more important than inertial forces. This occurs as the turbulent mechanical energy generated at the outer scale is transferred to eddies of smaller and smaller scales until the inner scale is reached, where it is converted into heat. For atmospheric turbulence near the ground, the inner scale for refractive index fluctuations can vary between 1 and 25 mm [8-10].

At this point, it would be profitable to reformulate the problem into Fourier space, since it is in this form that wave propagation calculations are performed. We can use a Fourier transform to turn a random field of refractive index fluctuations in ordinary space, $n(\bar{x},t)$, into a complex random field in wavenumber space, $N(\bar{K},t)$ and to introduce the power spectrum,

$$\Phi_n(K) = \left\langle N^*(\bar{K},t) \cdot N(\bar{K},t) \right\rangle \tag{4}$$

where $K = |\vec{K}|$. Here, homogeneous, stationary and isotropic turbulence leads to a power spectrum that depends only on the magnitude of the wavenumber. Intuitively, the power spectrum represents the contribution of eddies with a size of the order of K^{-1} to the overall variance of the turbulent fluctuations, that is $\sigma_n^2 \propto \int \Phi_n(K) \mathrm{d}^3 K$.

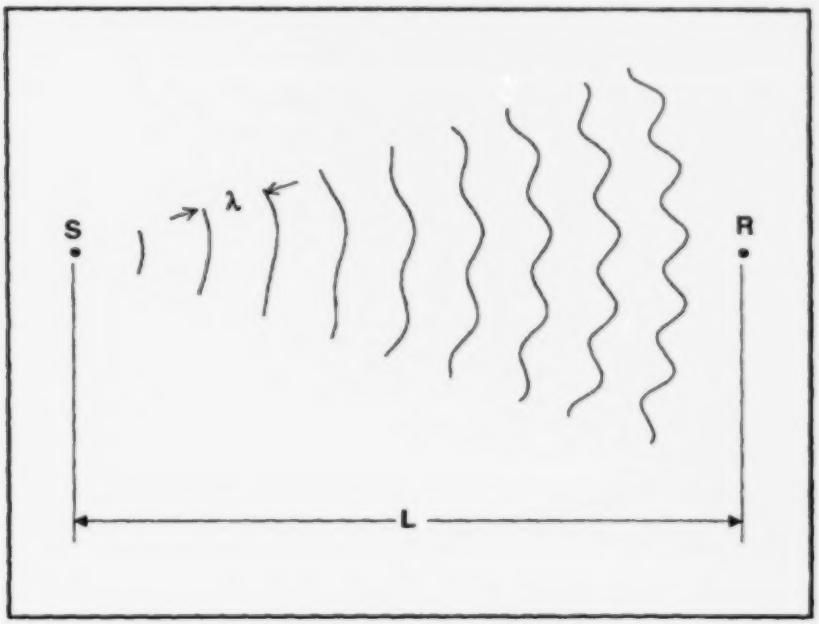

Figure 1. *A schematic illustration of a point source (S) emitting spherical waves through atmospheric turbulence to a point receiver (R). The source is a distance L from the receiver and the waves have a nominal wavelength λ. As the wavefronts propagate through the turbulence, they become progressively more distorted.*

The structure function of Eq. (3) leads to a power spectrum of the form [5],

$$\Phi_n(K) = 0.033 C_n^2 K^{-11/3} \tag{5}$$

However, this spectrum does not include the outer and inner scales mentioned previously. We therefore modify the spectrum in Eq. (5) by multiplying it with a function Γ that is equal to 1 in the inertial range, $2\pi/L_0 \ll K \ll 2\pi/l_0$, and tends towards zero as $K \to 0$ or $K \to \infty$. According to Churnside et al. [11-13], though, the outer scale has little effect on scintillation calculations. Therefore, we will only model the effect of the inner scale using their proposed function;

$$\Gamma(Kl_0) = \exp(-1.28K^2 l_0^2) + 1.45\exp\left\{-0.97\left[\ln(Kl_0) - 0.45\right]^2\right\}. \qquad (6)$$

The first term in Eq. (6) ensures that the turbulence spectrum is strongly attenuated for eddies much smaller than the inner scale. The second term causes Γ to be slightly greater than 1 for eddies in or around the inner scale. This is meant to simulate the "bump" around the inner scale in the turbulent refractive index spectrum observed by Champagne et al. [14] and Williams and Paulson [15].

2.2 The classical theory

The classical theory of wave propagation in a turbulent medium is what Clifford [16] called the theory developed around the early work of Chernov [17] and Tatarski [5]. This theory considers an incident electromagnetic wave, either planar or spherical, propagating over a certain distance through homogeneous, isotropic and stationary turbulence to a point receiver. From now on we will only consider spherical waves. Spherical waves emanating from a point source are depicted in Fig. 1. It also shows the cumulative effect of turbulence on the wave as it propagates. As the initial undistorted wavefront propagates, it meets turbulent eddies that act as lenses and distort the wavefront slightly, it consequently meets more eddies that distort it even more, and so on. The classical theory not only assumes a perfectly transparent atmosphere (no absorption or emission), it also assumes that single scattering adequately describes the wave propagation (this is called the *weak scattering* limit).

To understand what we mean by the weak scattering limit, it is convenient to divide the electromagnetic field of the emitted spherical wave of Fig. 1 (which we shall represent by the scalar field E without any loss of generality) into an unperturbed component, E_0, and a

perturbed component E', such that $E = E_0 + E'$. For simplicity, we will only consider the axis connecting the source **S** with the receiver **R**, denoted by the co-ordinate z, where $z = 0$ is the position of the source and $z = L$ the receiver. The unperturbed wave is given by,

$$E_0(z) = \frac{A_0}{z}\exp[i(kz + \phi_0)] \tag{7}$$

where $k = 2\pi/\lambda$ and λ is the wavelength of the unperturbed wave. In Eq. (7), we have dropped the time dependence $\exp[-ikct]$, where c is the speed of light. Therefore, as the wave is emitted, it is initially unperturbed, i.e. $E \approx E_0$ at $z \to 0$. After it has propagated over a short distance $\delta \ll L$, the wave has interacted with the turbulent eddies located in the interval $0 < z \le \delta$. The total wave at $z = \delta$ is now $E(\delta) = E_0(\delta) + E_1(\delta)$, where E_1 is the perturbed component produced by the scattering of the unperturbed wave, E_0, by the eddies between $0 < z \le \delta$. Since E_1 is the result of the scattering of E_0, we say that it represents the first-order scattering, or the single scattering. As the wave propagates from $z = \delta$ to $z = 2\delta$, both E_0 and E_1 are scattered by the eddies between $\delta < z \le 2\delta$. The wave is then given by $E(2\delta) = E_0(2\delta) + E_1(2\delta) + E_2(2\delta)$, where $E_1(2\delta)$ is the first-order scattering by the eddies between $0 < z \le 2\delta$, and $E_2(2\delta)$ is produced by the scattering of E_1 by the eddies between $\delta < z \le 2\delta$. Since E_2 is the scattering product of a scattering product, E_1, we say that it represents second-order, or double scattering. This process continues to produce third-order scattering, E_3, fourth-order scattering, E_4, and so on. The final perturbed component at the receiver is therefore given by

$$E'(L) = \sum_{n=1}^{\infty} E_n(L). \tag{8}$$

However, the first-order scattering is proportional to the standard deviation of the refractive index fluctuations, $E_1 \propto \sigma_n E_0$, whereas $E_2 \propto \sigma_n^2 E_0$, $E_3 \propto \sigma_n^3 E_0$, and so on. Therefore, if the refractive index fluctuations are sufficiently small, we need only consider the single scattering component (namely $E'(L) \approx E_1(L)$), or the weak scattering limit. For the weak

scattering limit to apply, however, not only must the turbulence be sufficiently weak, but the path L must not be too long, due to the cumulative nature of the scattering process.

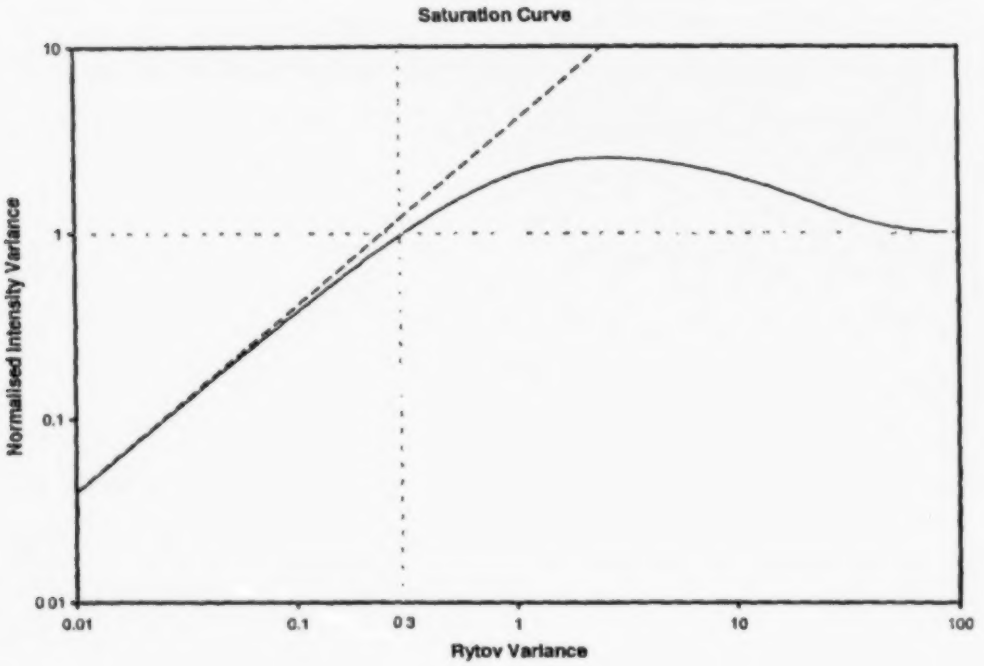

Figure 2. *The solid line is Tofsted's analytic expression for the normalised intensity variance, σ_I^2, as a function of Rytov's variance, σ_R^2. The dashed line is what we expect from the weak scattering theory. The vertical dotted line represents the threshold beyond which the weak scattering theory no longer holds. The horizontal dotted line is the asymptotic value of the normalised intensity variance in the limit of very strong scattering (saturation).*

This method of additive perturbations is known as the Born approximation. While it gives a clear physical explanation of turbulent scattering, it is only applicable for very weak turbulence and over very short paths. A less restrictive method, based on multiplicative perturbations is known as the Rytov approximation and was applied by Tatarski [5]. The Rytov approximation only requires that the refractive index fluctuations be smooth over the scale of a wavelength. Mathematically, this means that the perturbed wave is expressed as,

$$E(z) = \exp\left[\chi(z) + iS(z)\right] E_0(z) \tag{9}$$

where χ is the turbulent log-amplitude fluctuation, S is the turbulent phase fluctuation, and E_0 is the unperturbed incident wave, as before. Since it is scintillation that interests us, namely the variation of received intensity, we will concern ourselves mainly with the statistics of χ. The scintillation at the receiver is a function of the variance of the log-amplitude fluctuations σ_χ^2. For a spherical wave propagating through homogeneous Kolmogorov-type turbulence (with the spectrum of Eq. (5)) over a distance L to a point receiver, this variance is given by [16,18],

$$\sigma_\chi^2(L) = 0.124 k^{7/6} L^{11/6} C_n^2 . \tag{10}$$

Equation (10) is only valid for sufficiently weak scintillation, that is when $\sigma_\chi^2 < 0.3$ [18]. Also, for sufficiently weak scintillation, the log-amplitude obeys a Normal distribution to a good approximation. That means that the received intensity, $I = E^*(L)E(L)$, obeys a log-normal distribution and that the normalised intensity variance, σ_I^2, (better known as the *scintillation index*) satisfies,

$$\sigma_I^2 = \frac{\left\langle \left(I - \langle I \rangle\right)^2 \right\rangle}{\langle I \rangle^2} = \exp\left[4\sigma_\chi^2\right] - 1. \tag{11}$$

For small σ_χ^2 we can approximate Eq. (11) with,

$$\sigma_I^2 \approx 4\sigma_\chi^2 . \tag{12}$$

Although Eqs. (10) and (12) are only valid in the limit of weak scattering, it is useful to use Eq. (10) to define the Rytov variance; $\sigma_R^2 = 0.124 k^{7/6} L^{11/6} C_n^2$. This is because the Rytov variance can be used as a parameter that tells us when the weak scattering limit applies ($\sigma_R^2 < 0.3$) or when we are approaching the strong scattering limit ($\sigma_R^2 > 10$). It must be emphasised that beyond the weak scattering region, the Rytov variance no longer represents the log-amplitude variance, $\sigma_\chi^2 \neq \sigma_R^2$. An analytic expression for the normalised intensity variance as a function of the Rytov variance, $\sigma_I^2 = f\left(\sigma_R^2\right)$, given by Tofsted [19], is plotted in Fig. 2. While this expression is not perfect (see Tofsted [19] for its relative merits), it

nonetheless shows all the important features. In Fig. 2, we see that past $\sigma_R^2 = 0.3$, and even a little before, σ_I^2 is less than what we would expect from the weak scattering theory. This is because the multiple scattering that we neglected is starting to have an effect. The cumulative effect of the multiple scattering will be such that the coherence of the wave at the receiver will be destroyed. In the limit of very strong scattering (or "strong turbulence" according to Tofsted [19]), $\sigma_R^2 \to \infty$, the distribution of the normalised intensity will approach an exponential and $\sigma_I^2 \to 1$. In this limit, we say that the scintillation is *saturated*. Conversely, when the weak scattering theory applies (or when we have *weak turbulence*), we say that the scintillation is *unsaturated*. In between, $0.3 < \sigma_R^2 < 10$, we say that there is *intermediate saturation* (*or intermediate turbulence*).

2.3 A systems approach

A point source emitting to a point receiver is a highly idealised situation. A more realistic treatment is obtained when we consider an extended emitter and receiver as the input and output, respectively, of a linear system (though, as we shall see, this approach also has its share of idealisations, see Fante [20] for a detailed treatment).

As Fig. 3 shows, we expand on the point-source-point-receiver treatment of the previous section by considering a collection of point sources and point receivers. The point sources form an extended source and the point receivers form an extended receiver, and are both considered to be flat surfaces. Therefore, if we have an electric field at the source surface, $E_0(\bar{\rho}')$, where $\bar{\rho}' = (x', y', 0)$, then the Huygens-Fresnel principle states that each point of the source emits a spherical wave,

$$E(\bar{x}) \propto \left\{ \frac{k\, E_0(\bar{\rho}') \exp\left[ik|\bar{x} - \bar{\rho}'| \right]}{2\pi i |\bar{x} - \bar{\rho}'|} \right\} \cdot \exp\left[\chi(\bar{x}, \bar{\rho}') + iS(\bar{x}, \bar{\rho}') \right]. \qquad (13)$$

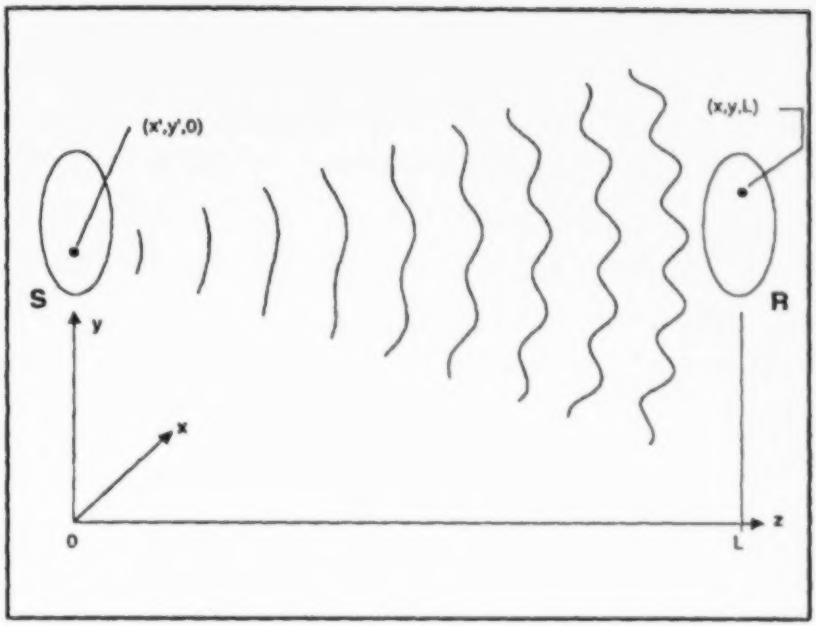

Figure 3. *A schematic illustration of the generalised Huygens-Fresnel principle used in the systems approach. The source (disk S) is modelled as a collection of point sources forming a surface on the plane* $z = 0$. *Each point source, labelled* $(x', y', 0)$, *emits a spherical wave that propagates through the turbulence and reaches the receiver. The receiver (disk R) is modelled as a collection of point receivers, labelled* (x, y, L), *forming a surface on the plane* $z = L$.

The terms inside the curly brackets of Eq. (13) represent the propagation of a spherical wave in a uniform medium. The exponential outside the curly brackets represents the distortion due to turbulence. The electric field at a point of the receiver, $\bar{\rho} = (x, y, L)$, is the sum of the spherical waves from all the point sources. This can be expressed as an integral over the surface area of the source, A', as

$$E(\bar{\rho}) = \int_S \mathrm{d}A' E_0(\bar{\rho}') h(\bar{\rho}, \bar{\rho}', L) \exp[\chi(\bar{\rho}, \bar{\rho}', L) + iS(\bar{\rho}, \bar{\rho}', L)] \qquad (14)$$

where $h(\bar{\rho}, \bar{\rho}', L)$ represents the propagation of a spherical wave in a vacuum with unit amplitude, originating from the point $\bar{\rho}' = (x', y')$ at the source plane ($z = 0$) and arriving at

the point $\vec{\rho} = (x, y)$ at the receiver plane ($z = L$), where the source and receiver planes are a distance L apart. The same notation holds for $\chi(\vec{\rho}, \vec{\rho}', L)$ and $S(\vec{\rho}, \vec{\rho}', L)$. Assuming that the source and the receiver are small compared to L, that is $\rho^2 = x^2 + y^2 \ll L$ and $(\rho')^2 = (x')^2 + (y')^2 \ll L$ (where $\vec{\rho}' = (0,0)$ and $\vec{\rho} = (0,0)$ are set at the centre of the source and receiver respectively), then h can be approximated as,

$$h(\vec{\rho}, \vec{\rho}', L) = \frac{k}{2\pi i L} \exp\left[ikL + i\frac{k}{2L}(\vec{\rho} - \vec{\rho}')^2\right] \tag{15}$$

where $(\vec{\rho} - \vec{\rho}')^2 = (x - x')^2 + (y - y')^2$. Equation (14) tells us that the received intensity at a point, $I(\vec{\rho}) = E^*(\vec{\rho}) \cdot E(\vec{\rho})$, is a double integral over the source surface (making it a quadruple integral). The average intensity is therefore,

$$\langle I(\vec{\rho}) \rangle = \int_{S_1} dA_1' \int_{S_2} dA_2' \langle E_0^*(\vec{\rho}_1') E_0(\vec{\rho}_2') \rangle \langle G^*(\vec{\rho}, \vec{\rho}_1', L) G(\vec{\rho}, \vec{\rho}_2', L) \rangle \tag{16}$$

where we used the simplification $G = h \cdot \exp[\chi + iS]$. Equation (16) assumes two things. First, that the electric field at the source may be random, hence the need to average over it. Second, that the randomness of the turbulence (expressed as a randomness in G) is independent of the source electric field. This simply means that the fluctuations of the electric field at the source have no effect on the turbulence between the source and the receiver.

At this point, we must say something about the statistics of the source. If the radiation coming from the source is due solely to thermal processes, like emissions from a blackbody, then the electric field at the source is taken as being completely *incoherent*. By this, we mean that there is no correlation between the electric field at one point of the source and the field at another point, no matter how close. We express this mathematically by

$$\langle E_0^*(\vec{\rho}_1') E_0(\vec{\rho}_2') \rangle = \frac{4\pi}{k^2} \delta(\vec{\rho}_1' - \vec{\rho}_2') \langle I_0(\vec{\rho}_1') \rangle \tag{17}$$

where I_0 is the intensity at the source. The normalization, $4\pi/k^2 = \lambda^2/\pi$, indicates the fact that the source field is correlated over distances smaller than about one wavelength. If the source were a laser, for instance, then Eq. (17) would not hold and the electric field would be

very strongly correlated over the entire surface of the source. Wolf [21] gives an interesting discussion on the coherence and incoherence of various optical systems.

Placing Eq. (17) in Eq. (16) enables us to eliminate one surface integral to give the following expression relating the average intensity at the receiver with that at the source:

$$\langle I(\bar{\rho})\rangle = \frac{4\pi}{k^2}\int_S dA' \langle I_0(\bar{\rho}')\rangle \langle |G(\bar{\rho},\bar{\rho}',L)|^2\rangle . \tag{18}$$

Equation (18) is directly analogous to Eq. (14), except that we are dealing with the average intensity rather than the instantaneous electric field. Using Eq. (15) we obtain,

$$\langle |G(\bar{\rho},\bar{\rho}',L)|^2\rangle = \frac{k^2}{4\pi^2 L^2}\langle \exp[2\chi(\bar{\rho},\bar{\rho}',L)]\rangle . \tag{19}$$

Assuming a perfectly transparent atmosphere, we require that, on average, no energy is absorbed or emitted, that is $\langle \exp[2\chi]\rangle = 1$ and Eq. (18) becomes,

$$\langle I(\bar{\rho})\rangle = \frac{1}{\pi L^2}\int_S dA' \langle I_0(\bar{\rho}')\rangle \tag{20}$$

which is identical to the result for a non-turbulent medium with an incoherent source. It is not obvious from Eq. (20) what the effects of turbulence are. Turbulence can have an important effect on scintillation, which is a second-order statistic for intensity (and therefore a fourth-order statistic for the electric field). Even for an incoherent source, the detailed treatment of scintillation from basic principles is quite complicated (see Fante [20]). We will omit such a derivation here, and simply cite the main result in the next section.

3. General integral

In this section, we will introduce without derivation the integral equations needed to describe scintillation for general conditions. The reader should consult [16,18,20] for more details. The main purpose of this section is to identify the relevant scales and qualitative properties of the integrals.

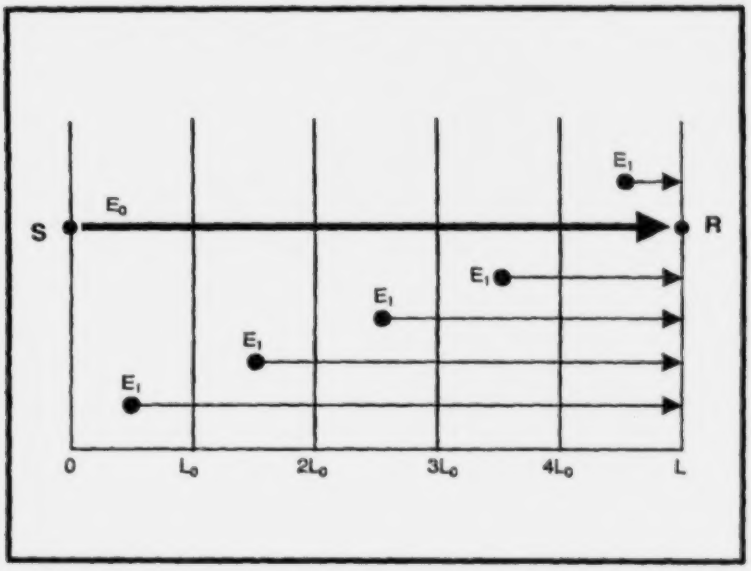

Figure 4. *A schematic illustration of the scattering process behind Eq. (21). The path between the source and the receiver is divided into many independent turbulent slabs of thickness equal to the outer scale of the turbulence* L_0. *Each slab interacts with the incident wave (fat arrow labelled* E_0*) to produce a first-order perturbation* E_1. *The scintillation at the receiver is produced by the sum of all the perturbations. It is assumed that each slab does not interact with the first-order perturbations from previous slabs.*

3.1 Weak scattering limit

As in the previous section, we will begin by considering the case of a point source and a point receiver in the weak scattering limit. The log-amplitude variance for this case can be given by the double integral,

$$\sigma_\chi^2 = 4\pi^2 k^2 L \int_0^1 \mathrm{d}r \int_0^\infty \mathrm{d}K K \Phi_n(K,r) \sin^2\left[\frac{K^2 Lr(1-r)}{2k}\right] \tag{21}$$

where $r = z/L$ is the normalised range and $\Phi_n(K,r)$ is the turbulence spectrum defined over a surface perpendicular to the path and located at r. Each surface can be thought of as a two-dimensional turbulent "screen" that interacts with the incident wave to produce a first-order perturbation wave. Equation (21) assumes that each screen is statistically independent from every other screen. This approximation is valid as long as $L_0 \ll L$, which is the case for long horizontal paths close to the ground, where $L_0 \leq 100\,\mathrm{m}$ and L is typically several kilometres. In fact, it would be better to picture the turbulence as composed of a large number of independent "slabs" of thickness L_0. This is illustrated in Fig. 4.

We will now assume that the turbulence has the form

$$\Phi_n(K,r) = 0.033 C_n^2(r) K^{-11/3} \tag{22}$$

which is identical to the Kolmogorov turbulence described in Eq. (5), except that the refractive index structure parameter is a function of r. At first sight this seems inconsistent as the K41 theory is built on the assumption of homogeneous turbulence, which means that C_n^2 must be constant. At this point we introduce the notion that the turbulence is only "locally homogeneous", which means that over scales significantly smaller than L_0 the turbulence acts as though it were homogeneous with a "constant" local value of C_n^2, but over scales significantly larger than L_0, turbulence parameters like C_n^2 are free to vary. Therefore, the function $C_n^2(r)$ must be relatively constant over normalised distances of the order $\Delta r \approx L_0/L$. It must be stressed that although the outer scale does not appear explicitly in Eq. (22), it plays an important indirect role in the formulation of the double integral of Eq. (21). Placing Eq. (22) in Eq. (21), we obtain

$$\sigma_\chi^2 = 1.303 k^2 L \int_0^1 \mathrm{d}r C_n^2(r) \int_0^\infty \mathrm{d}K K^{-8/3} \sin^2\left[\frac{K^2 \mu^2 r(1-r)}{4\pi}\right] \tag{23}$$

where $\mu = \sqrt{L\lambda}$ is the *Fresnel zone*, a very important length scale for what will follow. It is convenient to express the second integral in terms of the variable $y = K^2\mu^2 r(1-r)/(4\pi)$, which gives

$$\sigma_\chi^2 = 0.366 k^{7/6} L^{11/6} \left\{ \int_0^1 dr \left[r(1-r) \right]^{5/6} C_n^2(r) \right\} \left\{ \int_0^\infty dy\, y^{-11/6} \sin^2(y) \right\}. \qquad (24)$$

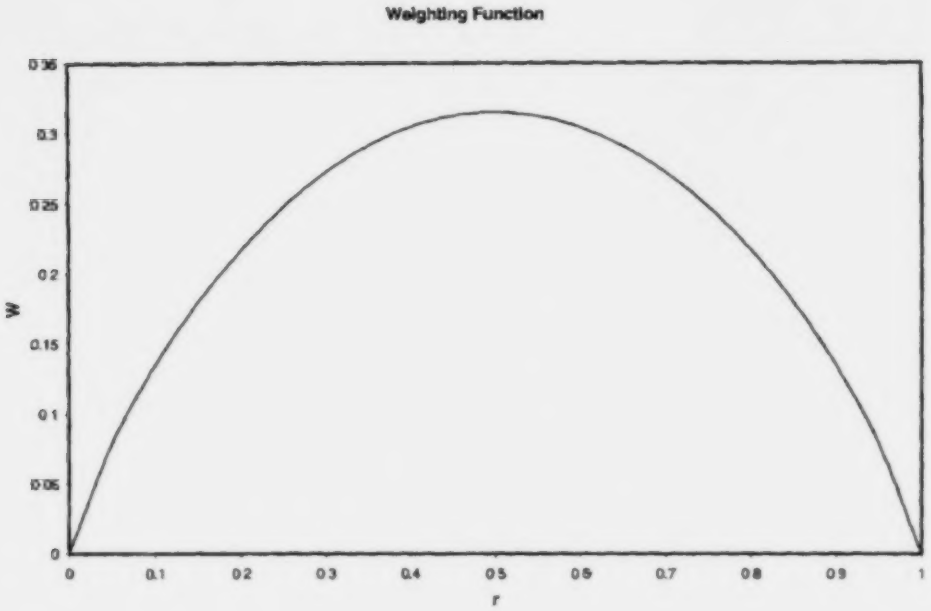

Figure 5. *The path weighting function as a function of the normalised range, r. This function indicates the sensitivity of the scintillation to the turbulence located at r.*

The substitution allows us to express the double integral as the product of two single integrals. The first integral in Eq. (24) is the integration of C_n^2 weighted according to the function $W(r) = \left[r(1-r) \right]^{5/6}$ over the path. This weighting function is a maximum in the middle of the path, $r = 0.5$, and zero at the ends (see Fig. 5). This means that it is the turbulence about midway between the source and the receiver that contributes the most to the scintillation.

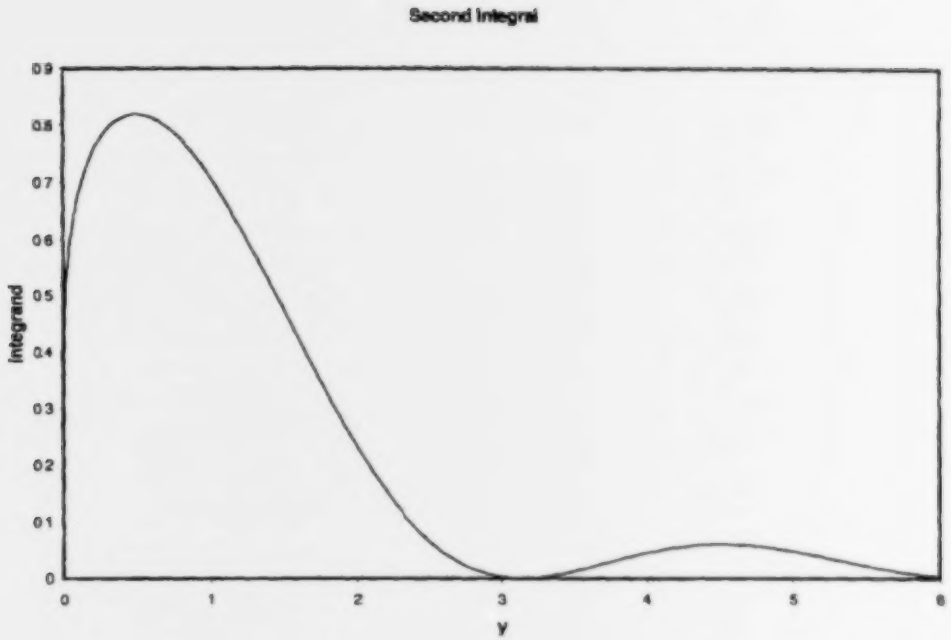

Figure 6. *The integrand of the second integral in Eq. (24). Note the main lobe with a maximum at about* $y \approx 0.5$, *followed by a series of much smaller lobes.*

The second integral in Eq. (24) has an integrand with a maximum at about $y \approx 0.5$, followed by a series of small lobes (see Fig. 6). Taking $r \approx 0.5$, on account of the path weighting function, we find that the second integrand maximises at around $K \approx \sqrt{8\pi}/\mu$, implying that turbulent eddies of about 1.25μ (approximately one Fresnel zone in size) contribute the most to the scintillation. Therefore, it is the Fresnel zone sized eddies about halfway between the source and the receiver that contribute the most to the scintillation. Born and Wolf [22] give a general discussion of Fresnel zones in optics and Clifford et al. [23] give a brief discussion on its role in scintillation. It is interesting to note that if we set C_n^2 to be a constant in Eq. (24) and evaluate it, we obtain $\sigma_I^2 = 0.124k^{7/6}L^{11/6}C_n^2 = \sigma_R^2$, the Rytov variance.

3.2 Intermediate regime

As mentioned previously, no good physical theory of saturation exists and we must use an empirically based approximation. Clifford et al. [23] formulated one such approximation that yields reasonable results (see also Hill and Clifford [24]). In this case, saturation is taken into account by modifying Eq. (21), as follows;

$$\sigma_\chi^2 = 4\pi^2 k^2 L \int_0^1 dr \int_0^\infty dK K \Phi_n'(K,r,l_0) \sin^2\left[\frac{K^2\mu^2 r(1-r)}{4\pi}\right] M(K,r,\Phi_n') \tag{25}$$

where $\Phi_n'(K,r,l_0) = \Gamma(Kl_0)\Phi(K,r)$ is a general turbulence spectrum that may include a nonzero inner scale. The saturation is described by the function M, which depends on the turbulence spectrum (and so indirectly on l_0 and $C_n^2(r)$) and is given as,

$$M(K,r,\Phi_n') = \exp\left(-4\pi^2 k^2 L \int_{\gamma K}^\infty dK' \Psi(K') \left\{1 - J_0\left[\frac{K'K\mu^2 r(1-r)}{2\pi}\right]\right\}\right) \tag{26}$$

where γ is a constant and

$$\Psi(K',r,l_0) = \int_{K'}^\infty dK'' \Phi_n'(K'',r,l_0). \tag{27}$$

For a general turbulence spectrum, Eqs. (26) and (27) are quite complicated. We can simplify them by assuming that C_n^2 is constant and $l_0 = 0$ (that is we assume a perfect Kolmogorov spectrum). In that case, Eq. (27) has a simple solution, and Eq. (26) can be written as,

$$M(K,r,\sigma_R^2) = \exp\left\{-\sigma_R^2 [r(1-r)]^{5/6} f(y)\right\} \tag{28}$$

where σ_R^2 is the Rytov variance (Eq. (10)), $y = K^2\mu^2 r(1-r)/4\pi$ as before, and

$$f(y) = 7.02 y^{5/6} \int_{\alpha y}^\infty d\xi \xi^{-8/3} \left[1 - J_0(\xi)\right] \tag{29}$$

where $\alpha = 2\gamma$. Setting $\alpha = 0.7$ gives a good fit to empirical scintillation data [23]. Assuming that C_n^2 is constant is reasonable for horizontal paths, while assuming a zero inner scale is reasonable only if $l_0 \leq \mu/7$ (Hill and Clifford [24]).

Equations (28) and (29) represent the way saturation will be modelled later in this work. It is therefore important to understand its limitations. Apart from the assumptions mentioned above, there is also the fact that as $\sigma_R^2 \to \infty$, we have $M \to 0$ (see Eq. (28)). This means that for very strong saturation, the scintillation index would asymptotically vanish ($\sigma_I^2 \to 0$) which is contrary to the result mentioned in Section 2.2, namely that $\sigma_I^2 \to 1$ in that limit. Therefore, the model used here only applies for weak or intermediate saturation, not strong saturation. In effect, the equations are thought to be valid for $0 \leq \sigma_R^2 < 10$.

3.3 Aperture averaging

Another important effect to be discussed is aperture averaging, both of the receiver and of the source. Following convention [12, 19, 25, 26], we will start by discussing the effect of the aperture averaging of the receiver on the scintillation assuming a point source. We define the characteristic function of the receiver, $\Theta(\bar{\rho})$, as equal to one for every point on the surface of the receiver and zero elsewhere. Then the power collected by the receiver is

$$I_A = \int \mathrm{d}A\, \Theta(\bar{\rho}) I(\bar{\rho}) \tag{30}$$

where due to the action of turbulence, the intensity I is a random function. We simplify by assuming that the receiver is a disk of diameter D (such that $\Theta(\bar{\rho}, D) = 1$ for $|\bar{\rho}| \leq D/2$, and $\Theta(\bar{\rho}, D) = 0$ for $|\bar{\rho}| > D/2$), and that the average intensity is constant over the area of the receiver, $\langle I(\bar{\rho}) \rangle = \langle I \rangle$. With these assumptions, the average of Eq. (30) yields

$$\langle I_A \rangle = (\pi/4) D^2 \langle I \rangle . \tag{31}$$

As we are interested in finding the scintillation index of I_A, we use Eq. (30), to give

$$\sigma_A^2 = \frac{\left\langle \left(I_A - \langle I_A \rangle\right)^2 \right\rangle}{\langle I_A \rangle^2} = \frac{16}{\pi^2 D^4} \int dA_1 \int dA_2 \Theta(\bar{\rho}_1, D)\Theta(\bar{\rho}_2, D) C_I(\bar{\rho}_1, \bar{\rho}_2) \tag{32}$$

where $C_I(\bar{\rho}_1, \bar{\rho}_2)$ is the intensity correlation function,

$$C_I(\bar{\rho}_1, \bar{\rho}_2) = \frac{\left\langle [I(\bar{\rho}_1) - \langle I \rangle][I(\bar{\rho}_2) - \langle I \rangle] \right\rangle}{\langle I \rangle^2} \tag{33}$$

where it is clear that for $\bar{\rho}_1 = \bar{\rho}_2$, Eq. (33) gives the scintillation index. Furthermore, assuming that the intensity correlation only depends on the distance between the two points, we have $C_I(|\bar{\rho}_1 - \bar{\rho}_2|)$. Then using the variables $\bar{q} = \bar{\rho}_1 - \bar{\rho}_2$ and $\bar{X} = (1/2)(\bar{\rho}_1 + \bar{\rho}_2)$ we can rewrite Eq. (32) as [24],

$$\sigma_A^2 = \frac{32}{\pi D^4} \int_0^D dq \left[q\, K_0(q, D) C_I(q) \right] \tag{34}$$

where

$$K_0(q, D) = \int d^2 \bar{X}\, \Theta\left(\bar{X} + \bar{q}/2, D\right)\Theta\left(\bar{X} - \bar{q}/2, D\right). \tag{35}$$

For a circular aperture, this gives

$$\begin{aligned} K_0(q, D) &= \frac{D^2}{2}\left\{ \cos^{-1}\left(\frac{q}{D}\right) - \left(\frac{q}{D}\right)\left[1 - \left(\frac{q}{D}\right)^2\right]^{1/2} \right\}, \quad \text{if } q \le D \\ &= 0, \qquad\qquad \text{if } q > D. \end{aligned} \tag{36}$$

The function $K_0(q, D)$, plotted in Fig. 7, represents the number of pairs of points a distance q apart where both points are on the receiving aperture. It is also the area of overlap between two circles of diameter D whose centres are displaced a distance q.

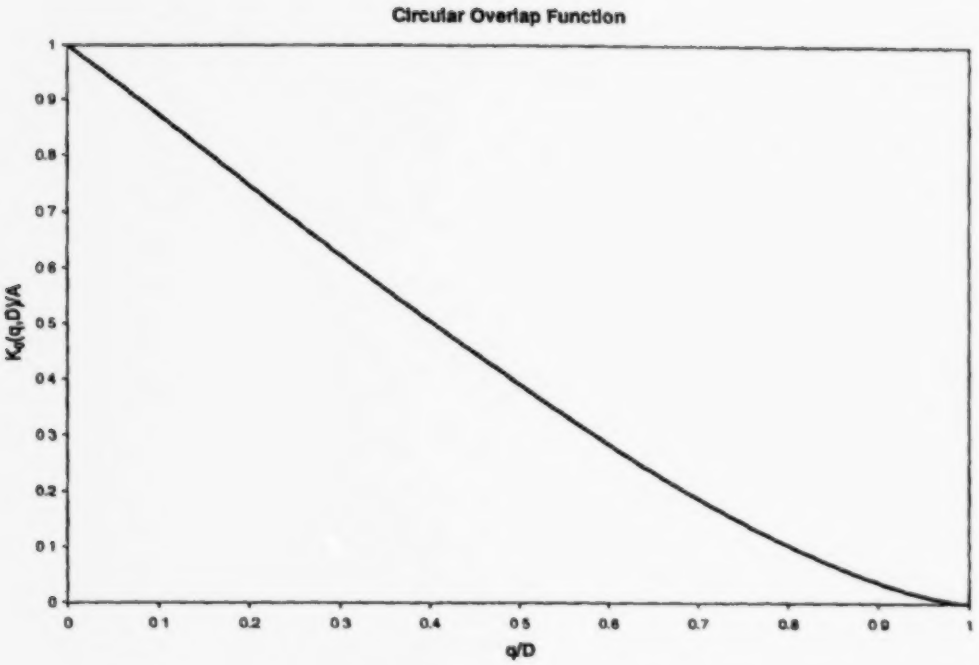

Figure 7. *The circular overlap function given by Eq. (36), normalised with respect to the area of the circle* $A = (\pi/4) D^2$ *and plotted with respect to its normalised argument.*

If the intensity fluctuations are log-normally distributed, then we have, in direct analogy with Eq. (11),

$$C_I(q) = \exp\left[4C_\chi(q)\right] - 1 \tag{37}$$

where $C_\chi(q) = \left\langle \left[\chi(\vec{\rho}) - \langle\chi\rangle\right]\left[\chi(\vec{\rho}+\vec{q}) - \langle\chi\rangle\right]\right\rangle$ is the log-amplitude covariance function. Furthermore, if the fluctuations are sufficiently small, we may approximate, as before, $C_I(q) \approx 4C_\chi(q)$. In that limit, Eq. (34) becomes,

$$\sigma_A^2 \approx \frac{128}{\pi D^4} \int_0^D dq \left[q K_0(q, D) C_\chi(q) \right]. \tag{38}$$

It is Eq. (38), or some version of it, that is most often used to determine the effects of aperture averaging. An analytic approximation for the log-amplitude covariance is given by Fried [27] and is plotted in Fig. 8.

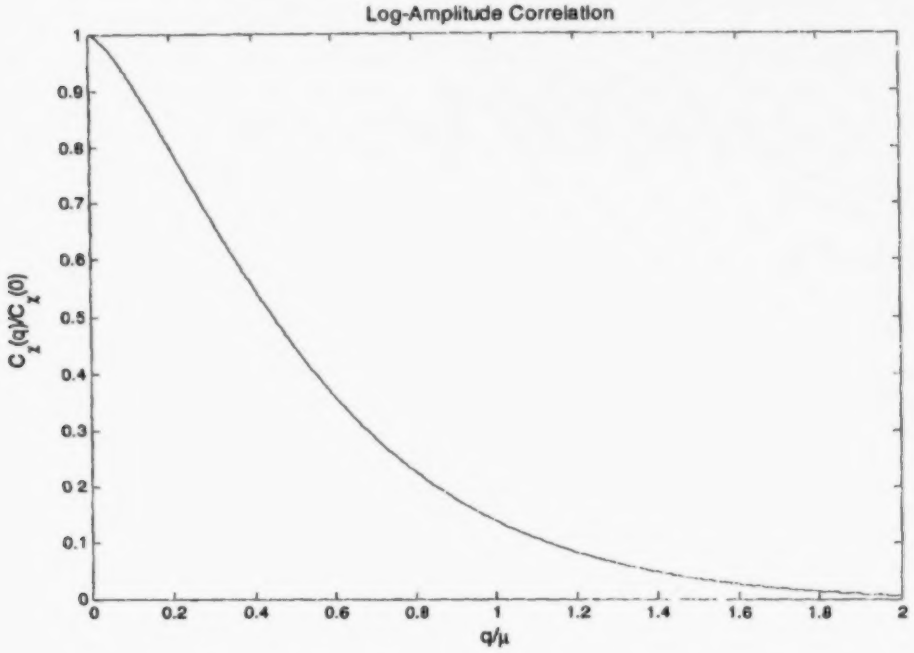

Figure 8. *The log-amplitude covariance function for spherical wave propagation through Kolmogorov turbulence according to Fried [27] with respect to the separation distance normalised by the Fresnel zone, q/μ.*

Figure 9 shows a comparison between the aperture averaged scintillation index using the exact exponential formula (Eq. (34) and Eq. (37)) and the scintillation index using the linear approximation (Eq. (38)) for various aperture diameters ($0 \le D < 1.75\mu$). Good agreement between the exponential and linear formulas is obtained for all diameters when the scintillation index is less or equal to 0.2. Beyond 0.2, we find that the linear formula underestimates the scintillation, and the underestimation worsens as the diameter gets larger. Therefore, if we used the linear formula to deduce a value of C_n^2 from a measured value of the scintillation index, the C_n^2 value could be significantly overestimated should the measured scintillation index be substantially greater than 0.2.

The log-amplitude covariance in the weak scattering limit for a spherical wave is given by the double integral [12, 26]

$$C_\chi(q) = 4\pi^2 k^2 L \int_0^1 dr \int_0^\infty dK K \Phi_n'(K, r, l_0) J_0(Krq) \sin^2\left[\frac{K^2 \mu^2 r(1-r)}{4\pi}\right]. \qquad (39)$$

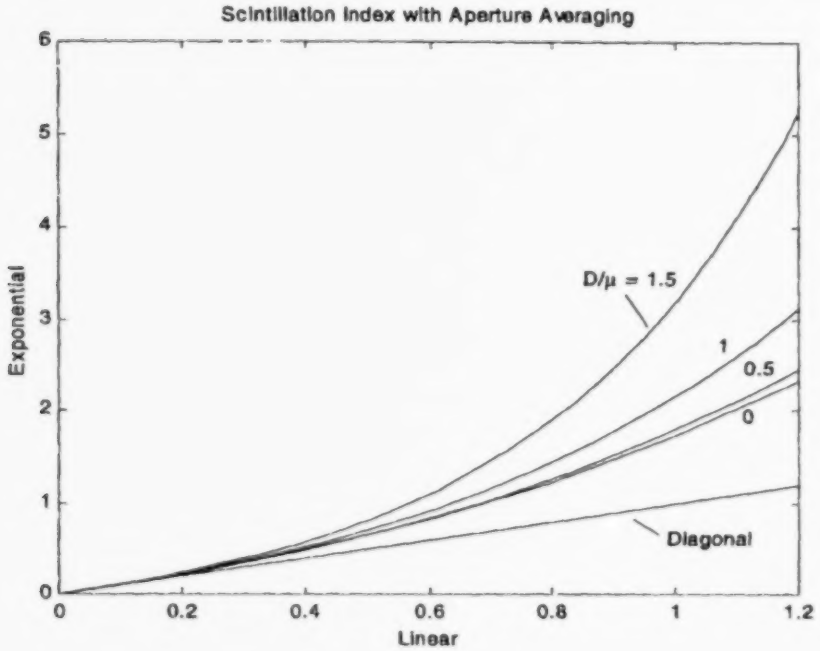

Figure 9. *A plot of the scintillation index using the exponential formula (Eq. (34) and Eq. (37)) as a function of the scintillation index evaluated using the linear approximation (Eq. (38)). Apart from the diagonal, there is also the point-receiver case ($D = 0$) as well as the cases of finite aperture ($D = 0.5\mu$, $D = \mu$ and $D = 1.5\mu$).*

Since $J_0(0) = 1$, setting $q = 0$ in Eq. (39) gives us Eq. (21), as expected. Placing Eq. (39) in Eq. (38) we obtain,

$$\sigma_A^2 = 16\pi^2 k^2 L \int_0^1 dr \int_0^\infty dK K \Phi_n'(K, r, l_0) B(KDr) \sin^2\left[\frac{K^2 \mu^2 r(1-r)}{4\pi}\right] \qquad (40)$$

where

$$B(KDr) = \frac{32}{\pi D^4}\int_0^D dq\left[qK_0(q,D)J_0(Krq)\right] = \left[\frac{2J_1(0.5KDr)}{0.5KDr}\right]^2. \tag{41}$$

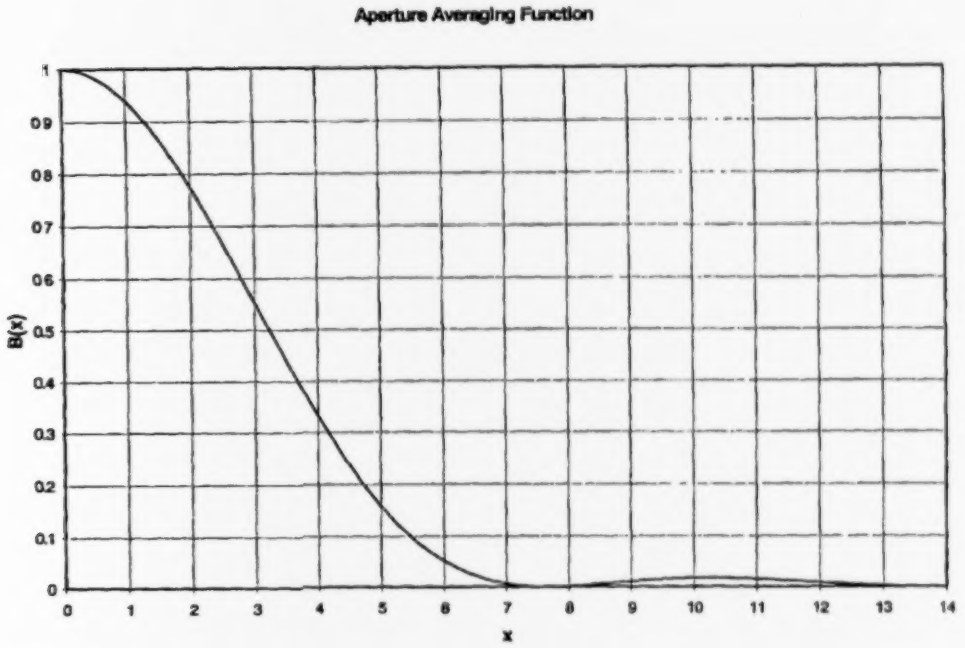

Figure 10. *A plot of the aperture averaging function* $B(x)$ *described by Eq. (41).*

Thus, Eq. (40) is essentially the same as Eq. (21) except that the function $B(KDr)$, which represents the effect of aperture averaging of the receiver, is included in the double integral.

The aperture averaging function is plotted in Fig. 10. In it, we see that $B(x)$ consists essentially of one lobe with the maximum at $x = 0$ and the half-power point ($B = 0.5$) at about $x \approx 3.2$. Therefore, for a given aperture $D > 0$, the receiver aperture averaging will

be most sensitive to turbulence close to the source ($r \to 0$), and/or of very small wavenumbers ($K \ll 2\pi D^{-1}$).

We can readily extend Eq. (40) to include a source with a nonzero diameter by inserting the function $B\left(KD_s(1-r)\right)$ to the double integral (from now on, the receiver diameter will be denoted by D_r for the sake of consistency). This result will not be derived but should be clear on physical grounds. As we saw in Sec. 2.3, the incoherence of the source means that we need only consider the intensity at the source surface, and not the electric field. Also, the transparency of the atmosphere means that the ray paths are reversible. Therefore, if the turbulence affects, in a certain way, a ray emitted from a point on the source and arriving at a point on the receiver, then it would affect, in the same way, a hypothetical ray emitted from that point on the receiver and arriving at the corresponding point on the source. We could then perform the same analysis for the emitted intensity at the source as we did for the intensity arriving at the receiver. Finally, upon including the effect of saturation into Eq. (40) we get,

$$\sigma_A^2 = 16\pi^2 k^2 L \int_0^1 dr \int_0^\infty dK K \Phi_n'(K, r, l_0) B(KD_r r) B\left(KD_s(1-r)\right) \times M\left(K, r, \sigma_R^2\right) \sin^2\left[\frac{K^2 \mu^2 r(1-r)}{4\pi}\right] \tag{42}$$

where $M\left(K, r, \sigma_R^2\right)$ is the saturation function given by Eq. (28) and by Eq. (29). It is important to note that this equation uses the linear approximation $C_I(q) \approx 4C_\chi(q)$. However, its range of validity extends beyond the limit seen in Fig. 9. This is because the saturation function reduces the underestimation caused by the linear approximation to an acceptable level. However, as we saw in section 3.2, the saturation function does not have the proper limit for very strong saturation, and so we only consider cases where $\sigma_R^2 < 10$. Equation (42) is the basic equation that we will analyse for the remainder of this report and whose general properties we will now investigate.

3.4 General properties

For what follows, it will be convenient to simplify Eq. (42) by assuming that C_n^2 is constant. Furthermore, it is easier to examine the correction factor $F = \sigma_A^2 / \left(4\sigma_R^2\right)$, such that in the limit of weak saturation with no inner scale and a point source and point receiver ($\sigma_R^2 \to 0$, $l_0 \to 0$, $D_s \to 0$ and $D_r \to 0$), we have $F \to 1$. It is also convenient to introduce a turbulence wavenumber normalised with respect to the Fresnel zone, $\kappa = K\mu$, as well as a normalised inner scale, $\lambda_0 = l_0 / \mu$, and normalised diameters, $\alpha_r = D_r / \mu$ and $\alpha_s = D_s / \mu$;

$$F(\alpha_s, \alpha_r, \lambda_0, \sigma_R^2) = C \int_0^1 \mathrm{d}r \int_0^\infty \mathrm{d}\kappa H(\kappa, r) \Gamma(\kappa\lambda_0) B(\kappa\alpha_r r) B\left(\kappa\alpha_s (1-r)\right) M\left(\kappa, r, \sigma_R^2\right) \quad (43)$$

where $C = 48.596$ is a normalisation constant, and $H(\kappa, r) = \kappa^{-8/3} \sin^2\left[\kappa^2 r(1-r)/4\pi\right]$ is the Fresnel zone function which has a maximum for turbulent eddies approximately one Fresnel zone wide ($\kappa \approx 1$) located about midway between the source and receiver ($r \approx 0.5$). The first thing to notice is that the correction factor is symmetric with respect to interchanging the source with the receiver. Namely, if we replace α_s in Eq. (43) with α_r and vice versa, and r with $1-r$, then by inspection we can see that Eq. (43) remains unchanged. This means that $F\left(\alpha_s, \alpha_r, \lambda_0, \sigma_R^2\right) = F\left(\alpha_r, \alpha_s, \lambda_0, \sigma_R^2\right)$. This property not only constrains the analytic formula we wish to find, but also allows us to avoid unnecessary computations in the numerical analysis.

The second thing to consider is the effect of large apertures on the sensitivity of F to saturation and a nonzero inner scale. Let's begin with saturation. For a given value of κ, we can see from Eq. (28) that the saturation function is equal to one at the end-points ($M\left(\kappa, 0, \sigma_R^2\right) = M\left(\kappa, 1, \sigma_R^2\right) = 1$). Therefore, the saturation function has its greatest effect in the middle of the path. However, for a large enough source ($\kappa\alpha_s \gg 1$), the corresponding aperture averaging function will be very small at the source ($r = 0$, $B(\kappa\alpha_s) \ll 1$). Similarly, if the receiver is sufficiently large, then its aperture averaging function will be very

small at the receiver (for $\kappa\alpha_r \gg 1$ at $r=1$, then $B \ll 1$). The product of the aperture averaging functions will attain a minimum around the middle of the path for wavenumbers $\kappa \gg \alpha_s^{-1}$ and $\kappa \gg \alpha_r^{-1}$, exactly where the saturation function has its largest effect. Therefore, if the source and receiver are large enough, they can effectively 'mask' the effect of the saturation function. Wang et al. [28] have determined that this happens whenever

$$\alpha_r + \alpha_s > 1.95\left(\sigma_R^2\right)^{3/5}. \tag{44}$$

Therefore, whenever Eq. (44) is satisfied, the correction factor will approach the value for no saturation, i.e. $F\left(\alpha_s, \alpha_r, \lambda_0, \sigma_R^2\right) \approx F\left(\sigma_s, \sigma_r, \lambda_0, 0\right)$.

We now turn our attention to the inner scale (while bearing in mind that we require $\lambda_0 \leq 7^{-1} \approx 0.143$ for the saturation function to be accurate). The inner scale function $\Gamma\left(\kappa\lambda_0\right)$ only has an effect for wavenumbers $\kappa \geq \lambda_0^{-1}$. In order to mask the inner scale effect, the product of the aperture averaging functions must be very small at those wavenumbers. Applying the same reasoning as in Wang et al. [28], we obtain the condition,

$$\frac{1}{2\lambda_0} > \frac{1}{\alpha_r} + \frac{1}{\alpha_s} \tag{45}$$

for the inner scale effect to be masked by the apertures. The first thing to notice is that Eq. (45) does not depend on the Fresnel zone (unlike Eq. (44)). Furthermore, using the normalisation formula, we can rewrite the inner scale condition as

$$\frac{1}{2} > \frac{l_0}{D_s} + \frac{l_0}{D_r}. \tag{46}$$

A striking feature of Eq. (46) is that for a nonzero inner scale and a point source ($D_s = 0$), the inner scale condition is violated for any value of receiver diameter. Therefore, for a point source a nonzero inner scale may always have an effect, though not necessarily a large one. This contrasts with the saturation condition, where for a point source, the effect of saturation may be masked provided the receiver diameter is large enough. The inner scale is typically of the order of 1 cm. In this work, we will concern ourselves with systems where both the source and the receiver diameters are of the order of 10 cm or greater. For such systems, the

inner scale condition is clearly satisfied and we may neglect inner scale effects, i.e. $F\left(\alpha_s,\alpha_r,\lambda_0,\sigma_R^2\right)\approx F\left(\alpha_s,\alpha_r,0,\sigma_R^2\right)$. Actually, for a system with $D_s=D_r=20$ cm an inner scale of less than 1 cm produces negligible variations in F while an inner scale of 2.5 cm increases it by about 20% [10]. But an error of 20% is readily accepted in exchange for this simplification. Consequently, in this report, we will neglect inner scale effects and assume $F\left(\alpha_s,\alpha_r,\sigma_R^2\right)=F\left(\alpha_s,\alpha_r,0,\sigma_R^2\right)$.

4. Correction factor derivation

In this section we will derive an analytic formula for the correction factor $F(\alpha_s, \alpha_r, \sigma_R^2)$ by examining the output of MATLAB routines that perform simple trapezoidal integrals (see Ref. [29]). We begin by considering the weak scattering limit, and then we look at the case of intermediate saturation.

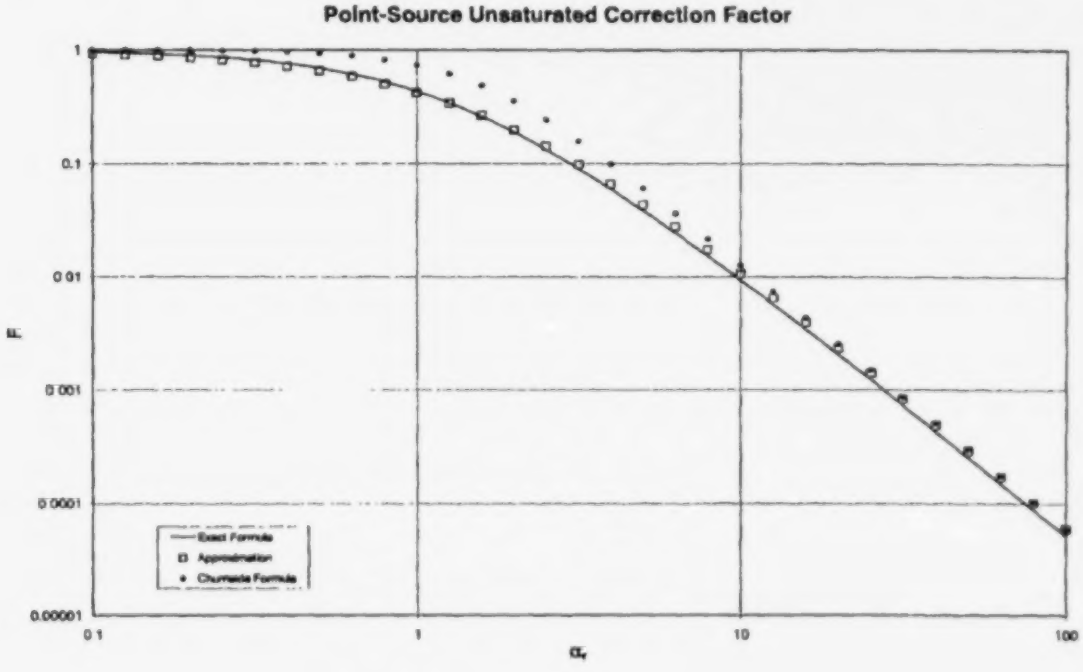

Figure 11. The solid line is the exact formula for the correction factor for a point source, zero inner scale and no saturation. The boxes are the approximation given by Eq. (47), and the small black circles are Chumside's formula [12, 26].

4.1 Weak scattering limit

In this section we will attempt to express the unsaturated correction factor $F(\alpha_s, \alpha_r, 0)$ in terms of the point source unsaturated correction factor, $F_S(\alpha_r) = F(0, \alpha_r, 0)$. This is

because F_S has been extensively studied in the literature and is therefore a good place to start. We propose the approximation,

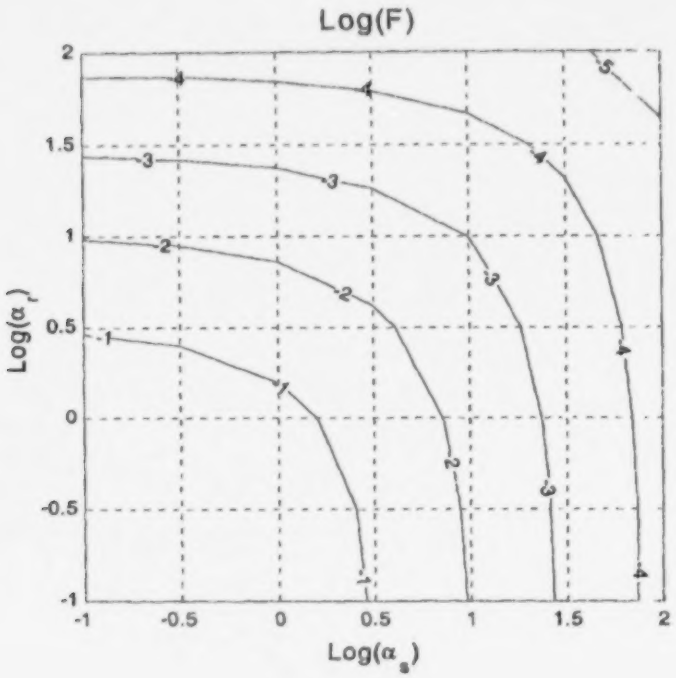

Figure 12. *A contour plot of the logarithm of the exact correction factor as a function of the source and receiver diameters.*

$$F_S(\alpha_r) = \frac{1}{1+\alpha_r^{7/6}+0.362\alpha_r^{7/3}}. \tag{47}$$

Equation (47) is plotted in Fig. 11. It displays a reasonable fit, underestimating the exact formula by about 5% at $\alpha_r \approx 0.5$ (-0.25 dB) and overestimating it by about 15% (0.65 dB) for $\alpha_r \approx 100$. It is important to note that the approximation in Eq. (47) is a modification of the formula given by Churnside [26,27] and Tofsted [19], $F_S = \left[1+0.362\alpha_r^{7/3}\right]^{-1}$, also plotted in Fig. 11. This formula is 86% (2.7 dB) greater than the exact formula at $\alpha_r \approx 1.6$. The modification is subject to the constraint that its exponent must be greater than one to

ensure that the derivative of the correction factor vanishes for a point-receiver, $F_s'(0)=0$, a property which follows from the aperture averaging functions in Eq. (43).

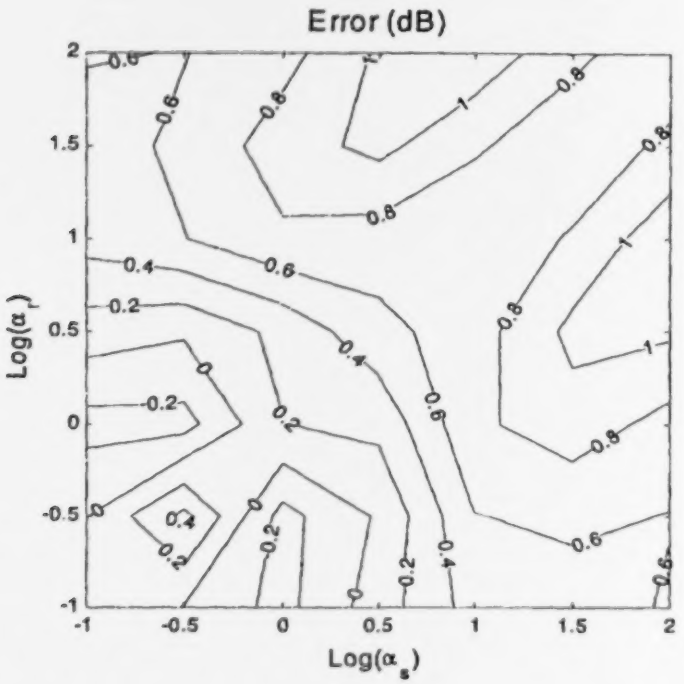

Figure 13. A contour plot of the difference, in dB, between the approximation given by Eq. (47) and (48), and the exact correction factor.

As can be seen in Fig. 13, a good approximation with respect to the exact formula, plotted in Fig. 12, is obtained by setting $F(\alpha_s,\alpha_r,0)=\left[1+\alpha_1^{7/6}+0.362\alpha_2^{7/3}\right]^{-1}$, where Eq. (47) has been modified by introducing the effective diameters, α_1 and α_2, defined by

$$\alpha_n=\sqrt{\alpha_s^2+\alpha_r^2+c_n\alpha_s\alpha_r} \tag{48}$$

where a good fit has been obtained by setting $c_1=-1.97$ and $c_2=6$. As noted earlier, the symmetry of the correction factor with respect to the source and receiver diameters allows us to evaluate only half the points of the grid needed to draw the contour plots. Figure 13 shows

that over the range of diameters considered, the error of the approximation with respect to the exact formula is no more than 1.2 dB (30%) and no less than –0.25 dB (-5%). The greatest error forms lobes centred around $\alpha_s \approx 10$, $\alpha_r \approx 100$, and $\alpha_s \approx 100$, $\alpha_r \approx 10$.

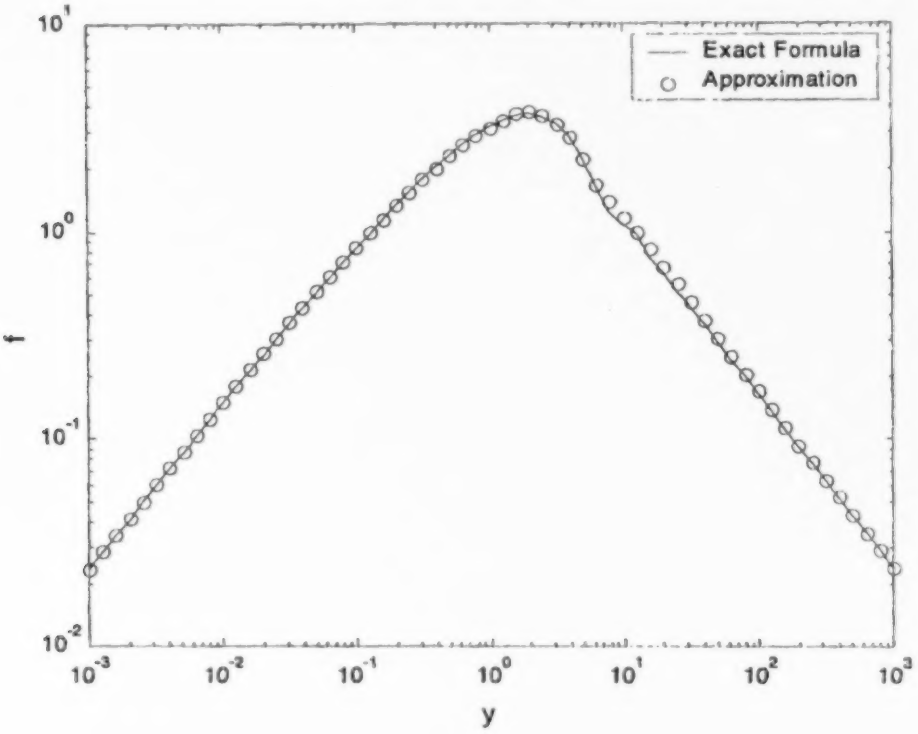

Figure 14. *The solid line is the exact evaluation of the integral function in Eq. (29). The circles represent the approximation given by Eq. (49).*

4.2 Intermediate regime

In order to obtain a workable program that includes saturation, it is necessary to find an analytic approximation to the integral in Eq. (29). This approximation will prevent our double integral from turning into a triple integral. A good approximation is found by setting (see Fig. 14),

$$\log f = \log(7.9) - \left\{0.11 + \left[(5/6)\log y\right]^2\right\}^{1/2} + 0.65(\log y - 0.15)\exp\left[-2|\log y - 0.15|\right] - 0.75(\log y - 0.7)\exp\left[-|(\log y - 0.7)/0.15|\right] \quad . \tag{49}$$

Next, we model the effect of saturation with the function $G(\alpha_s, \alpha_r, \sigma_R^2)$, which will multiply the unsaturated correction factor, $F(\alpha_s, \alpha_r, \sigma_R^2) = F_S(\alpha_{eff}) G(\alpha_s, \alpha_r, \sigma_R^2)$. Of course, we require that $G(\alpha_s, \alpha_r, 0) = 1$, by definition. Furthermore, in keeping with the condition described by Eq. (44), we also require that, in our model, $G(\alpha_s, \alpha_r, \sigma_R^2) = G(\alpha_s + \alpha_r, \sigma_R^2)$.

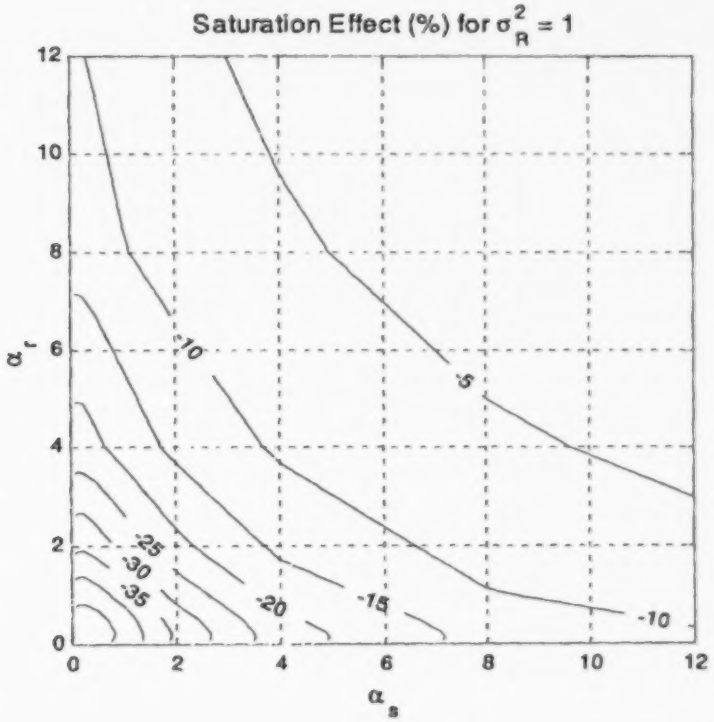

Figure 15. A contour plot of the effect of saturation with respect to no saturation in percent, $100(G-1)$, estimated by numerical integration for the case where $\sigma_R^2 = 1$.

Figure 15 gives us an example of the effect of saturation with a Rytov variance equal to one. In this case, the contour lines from –40% to –20% display the roughly straight diagonal lines we would expect from Eq. (44). We also notice significant deviations for the contours less than –40% and greater than –20%; however, these lines only account for an error of 5% in the assumption that G only depends on $\alpha = \alpha_s + \alpha_r$, as can be seen in Fig. 16. The function G, evaluated along one of the axis ($\alpha_s = \alpha$ and $\alpha_r = 0$) is about 5% higher than the function evaluated along the diagonal, $\alpha_s = \alpha_r = 0.5\alpha$, for $\alpha < 4$, and about 5% lower for $\alpha > 4$.

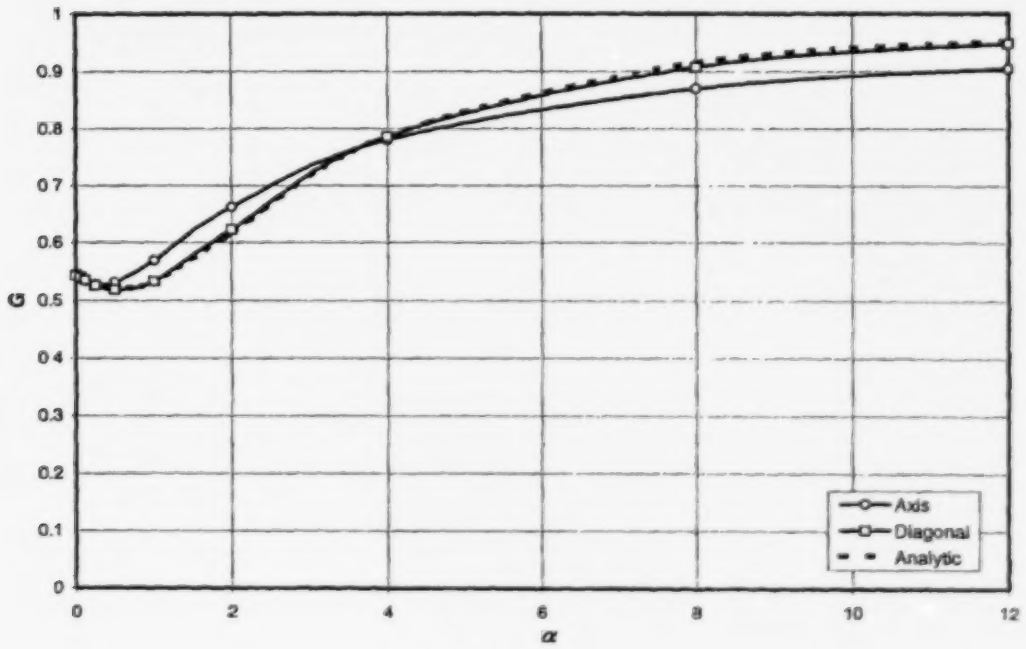

Figure 16. *Two cross-sections of the saturation effect function G for the case $\sigma_R^2 = 1$. The solid line with the circles is the cross-section along one of the axis of the contour plot in Fig. 15, that is $\alpha = \alpha_s$ and $\alpha_r = 0$, or vice-versa. The line with the squares is the cross-section along the diagonal, $\alpha_s = \alpha_r = 0.5\alpha$. The dotted line is the analytic formula.*

The grey line in Fig. 16 is our analytic approximation for G, given as

$$G\left(\alpha,\sigma_R^2\right)=\frac{A+\left(\alpha/2.5\right)^{7/3}}{1+b\alpha+\left(\alpha/2.5\right)^{7/3}} \tag{50}$$

where $A=G\left(0,\sigma_R^2\right)$ and b are both functions of σ_R^2. A good approximation for A and b over the range $0\le\sigma_R^2<10$ is

$$A=\exp\left[-0.6601\sigma_R^2+0.0518\left(\sigma_R^2\right)^2-0.0009\left(\sigma_R^2\right)^3-0.00009\left(\sigma_R^2\right)^4\right]; \tag{51}$$

and

$$b=0.1294\left(\sigma_R^2\right)^{1.2342}. \tag{52}$$

Figure 16 shows that the analytic function described by Eqs. (50) to (52) follows the diagonal function rather than the axis function. This is generally true over the range of the Rytov variance considered. Therefore, the analytic saturation effect function should slightly overestimate the effect of saturation for $\alpha<4$, and slightly underestimate it for $\alpha>4$.

5. Summary and discussion

In this work, we have attempted to describe the scintillation index of a system with nonzero source and receiver apertures and with significant saturation (i.e. $\sigma_R^2 \geq 1$), using simple analytic formulas. These formulas were developed using a combination of theoretical considerations and empirical form fitting. We have sought to describe the scintillation with a correction factor, F, such that;

$$\sigma_I^2 = 4F\left(\alpha_r, \alpha_s, \lambda_0, \sigma_R^2\right)\sigma_R^2 \tag{53}$$

where $\sigma_R^2 = 0.124k^{7/6}L^{11/6}C_n^2$. The correction factor is decomposed into two terms as

$$F\left(\alpha_r, \alpha_s, \lambda_0, \sigma_R^2\right) = F_S\left(\alpha_1, \alpha_2\right)G\left(\alpha_s + \alpha_r, \sigma_R^2\right) \tag{54}$$

where

$$F_S\left(\alpha_1, \alpha_2\right) = \frac{1}{1 + \alpha_1^{7/6} + 0.362\alpha_2^{7/3}} \tag{55}$$

takes into account the aperture averaging of the source and the receiver, with $\alpha_n = \sqrt{\alpha_s^2 + \alpha_r^2 + c_n\alpha_s\alpha_r}$, $c_1 = -1.97$ and $c_2 = 6$. The saturation effect function, G, is given as

$$G\left(\alpha, \sigma_R^2\right) = \frac{A + \left(\alpha/2.5\right)^{7/3}}{1 + b\alpha + \left(\alpha/2.5\right)^{7/3}} \tag{56}$$

where $b = 0.1294\left(\sigma_R^2\right)^{1.2342}$, and the function $A = A\left(\sigma_R^2\right)$ is given by Eq. (51).

Now, we must address the applicability and accuracy of the above formulas. The first thing to notice is that the normalized inner scale λ_0 is dropped in the decomposition of Eq. (54). This assumes that the source and receiver diameters are large enough so that the condition given by Eq. (46) applies (i.e. that the source and receiver can mask the inner scale effect). It also

assumes that $\lambda_0 \leq 1/7$, so that the saturation function in Eq. (28) and (29), on which G is based, remains valid.

As for accuracy, the largest error is introduced by using the effective aperture diameter approximation in the unsaturated point source function $F_S(\alpha_1, \alpha_2)$, which can be as much as 30% too large for certain values of the source and receiver diameters (see Fig. 13). In that region, the saturation effect function can also add as much as 5% to the error. However, this is partially offset by neglecting the inner scale, which can cause correction factor values that are as much as 20% too low for reasonable estimates of the inner scale, source and receiver diameters. Therefore, it would seem that 35% is the maximum error that we can expect from the proposed formulation over the considered range of diameters, saturation and inner scale. Assuming that typical parameters vary within the ranges $3 \leq L \leq 30\,\text{km}$, $0.5 \leq \lambda \leq 10\,\mu\text{m}$, $20 \leq D_s \leq 50\,\text{cm}$, and $10 \leq D_r \leq 20\,\text{cm}$, we obtain the ranges for the normalised diameters, $0.365 \leq \alpha_s \leq 12.92$ and $0.183 \leq \alpha_r \leq 5.168$, which we simplify by considering the range $0.15 < \alpha_s < 15$ and $0.15 < \alpha_r < 15$. Within this range, we see in Fig. 13 a maximum error of 20% (0.8 dB), thereby giving us a maximum error of 25% for typical systems.

Finally, it must be stressed that the decomposition in Eq. (54) allows us to take a 'modular' approach to the problem. For instance, we can modify how we model aperture averaging by changing F_S and α_n while leaving the saturation effect, G, unchanged. This can be a useful property when designing computer simulations.

6. Conclusions

In this report, we have examined the scintillation index from an incoherent source with an arbitrary aperture diameter, measured by an incoherent receiver with an arbitrary diameter, for weak to intermediate turbulence. Mathematically, the scintillation index is described by a triple integral. We have defined a correction factor that converts the Rytov variance into the scintillation index measured by an optical system. The correction factor is a function of the normalised source and receiver diameters, and the Rytov variance, which we have modelled with analytic functions. Provided that the inner scale of turbulence is sufficiently small, that the normalised diameters do not exceed 100 and that the Rytov variance does not exceed 10, the correction factor can be modelled to within a maximum error of 35% (or 1.3 dB) of its actual value. It must be emphasised that even if the analytic functions matched the triple integral perfectly, they would still only be as good as the underlying physical assumptions. For example, they could not model cases where the refractive index structure constant $C_n^2(r)$ or the inner scale $l_0(r)$ varied significantly with range.

The proposed correction factor has been presented as the product of two functions. The first function, F_S, represents the effect of source and receiver aperture averaging (and, consequently, is only a function of the normalised aperture diameters), while the second function, G, represents the effect of saturation (and depends on the Rytov variance as well as the normalised diameters). This decomposition introduces an additional small error of about 5%, but allows us to treat the different physical effects contributing to the correction factor separately. For instance, the parameters c_1 and c_2 characterising F_S (see Eqs. (47) and (48)) can be altered to achieve a better fit to empirical scintillation data without affecting G. Alternatively, the effect of saturation can be "turned-off", for whatever reason, simply by setting $G=1$. This modularity is extremely advantageous to integrated numerical models like IRBLEM, where the different physical effects can be handled by separate functions (computer modules), which can subsequently be altered without affecting the rest of the model.

7. References

1. Dion, D., Gardenal, L., Gilbert, J., Forand, L., Duffy, M., Lahaie, P. and Potvin, G., "IR Boundary Layer Effects Model (IRBLEM)", IRBLEM documentation version 3.6, 2001.

2. Kolmogorov, A.N., "The Local Structure of Turbulence in Incompressible Viscous Fluid for very large Reynolds Numbers", Dokl. Akad. Nauk SSSR, 30, pp. 301-304, 1941.

3. Kaimal, J. C. and Finnigan, J. J., "Atmospheric Boundary Layer Flows", Oxford University Press, Oxford, pp. 289, 1994.

4. Frisch, U., "Turbulence", Cambridge University Press, Cambridge, pp. 310, 1995.

5. Tatarski, V. I., "Wave Propagation in a Turbulent Medium", McGraw-Hill, New York, pp. 285, 1961.

6. Weichel, H., "Laser Beam Propagation in the Atmosphere", TT3, SPIE Optical Engineering Press, Bellingham, pp. 98, 1990.

7. Tofsted, D. H., "Turbulence Simulation: Outer Scale Effects on the Refractive Index Spectrum", ARL-TR-548, Nov. 2000, UNCLASSIFIED.

8. Trépanier, F. and Hutt, D. L., "Scintillation Measurements using the SCINTEC SLS 20 Scintillometer", DREV M-3194/94, May 1994, UNCLASSIFIED.

9. Hutt, D. L., "Modeling and Measurements of Atmospheric Optical Turbulence over Land", Opt. Eng., 38(8), pp. 1288-1295, 1999.

10. Frederickson, P. A., Davidson, K. L., Zeisse, C. R. and Bendall, C. S., "Estimating the Refractive Index Structure Parameter (C_n^2) over the Ocean Using Bulk Methods", J. Appl. Meteorol., 39(10), pp. 1770-1783, 2000.

11. Churnside, J. H., "A Spectrum of Refractive Turbulence in the Turbulent Atmosphere", J. Mod. Opt., 37(1), pp. 13-16, 1990.

12. Churnside, J. H., "Aperture Averaging of Optical Scintillations in the Turbulent Atmosphere", Appl. Opt., 30(15), pp. 1982-1994, 1991.

13. Churnside, J. H., Lataitis, R. J. and Wilson, J. J., "Two-color Correlation of Atmosphere Scintillation", Appl. Opt., 31(21), pp. 4285-4290, 1992.

14. Champagne, F. H., Friehe, C. A. and LaRue, J. C., "Flux Measurements, Flux Estimation Techniques, and Fine-Scale Turbulence Measurements in the Unstable Surface Layer Over Land", J. Atmos. Sci., 34(3), pp. 515-530, 1977.

15. Williams, R. M. and Paulson, C. A., "Microscale Temperature and Velocity Spectra in the Atmospheric Boundary Layer", J. Fluid Mech., 83(3), pp. 547-567, 1977.

16. Clifford, S. F., "The Classical Theory of Wave Propagation in a Turbulent Medium", In "Laser Beam Propagation in the Atmosphere", J. W. Strohbehn ed., Springer-Verlag, Berlin, pp. 9-43, 1978.

17. Chernov, L. A., "Wave Propagation in a Random Medium", Dover, New York, pp. 168, 1960.

18. Beland, R. R., "Propagation through Atmospheric Optical Turbulence", In "Atmospheric Propagation of Radiation", vol. 2, F. G. Smith ed., SPIE Optical Engineering Press, Bellingham, pp. 157-232, 1993.

19. Tofsted, D. H., "Empirical Modeling of Laser Propagation Effects in Intermediate Turbulence", SPIE Proc. Vol. 1487, Propagation Engineering: Fourth in a Series, pp. 372-381, 1991.

20. Fante, R. L., "Wave Propagation in Random Media: A Systems Approach", Progress in Optics XXII, E. Wolf ed., pp. 341-398, 1985.

21. Wolf, E., "Coherence and Radiometry", J. Opt. Soc. Am., 68(1), pp. 6-17, 1978.

22. Born, M. and Wolf, E., "Principles of Optics", Second Edition, Pergamon Press, New York, pp. 808, 1964.

23. Clifford, S. F., Ochs, G. R. and Lawrence, R. S., "Saturation of Optical Scintillation by Strong Turbulence", J. Opt. Soc. Am., 64(2), pp. 148-154, 1974.

24. Hill, R. J. and Clifford, S. F., "Theory of Saturation of Optical Scintillation by Strong Turbulence for Arbitrary Refractive-Index Spectra", J. Opt. Soc. Am., 71(6), pp. 675-686, 1981.

25. Fried, D. L, "Aperture Averaging of Scintillation", J. Opt. Soc. Am., 57, pp. 169-175, 1967.

26. Churnside, J. H., "Aperture-Averaging Factor for Optical Propagation through the Turbulent Atmosphere", NOAA Tech. Mem. ERL WPL-188, pp. 48, Nov. 1990.

27. Fried, D. L., "Propagation of a Spherical Wave in a Turbulent Medium", J. Opt. Soc. Am., 57, pp. 175-180, 1967.

28. Wang, T.-I., Ochs, G. R. and Clifford, S. F., "A Saturation-Resistant Optical Scintillometer to Measure C_n^2", J. Opt. Soc. Am., 68(3), pp. 334-338, 1978.

29. Press, W. H., Flannery, B. P., Teukolsky, S. A. and Vetterling, W. T., "Numerical Recipes", Cambridge University Press, Cambridge, pp. 818, 1988.

Bibliography

Andreas, E. L., ed., "Selected Papers on Turbulence in a Refractive Medium", SPIE Milestone Series vol. MS25, SPIE Optical Engineering Press, Bellingham, pp. 693, 1990.

Beran, M. J. and Oz-Vogt, J., "Imaging through Turbulence in the Atmosphere", Progress in Optics XXXIII, E. Wolf ed., pp. 341-398, 1994.

Clifford, S. F., Ochs, G. R. and Wang, T.-I., "Optical Wind Sensing by Observing the Scintillations of a Random Scene", Appl. Opt., 14(12), pp. 2844-2850, 1975.

Fante, R. L., "Electromagnetic Beam Propagation in Turbulent Media", Proc. IEEE, 63(12), pp. 1669-1692, 1975.

Fante, R. L., "Electromagnetic Beam Propagation in Turbulent Media: An Update", Proc. IEEE, 68(11), pp. 1424-1443, 1980.

Hill, R. J., "Review of Optical Scintillation Methods of Measuring the Refractive-Index Spectrum, Inner Scale and Surface Fluxes", Waves in Random Media, 2, pp. 179-201, 1992.

Hill, R. J. and Clifford, S. F., "Modified Spectrum of Atmospheric Temperature Fluctuations and its Application to Optical Propagation", J. Opt. Soc. Am., 68(7), pp. 892-899, 1978.

Kravtsov, Y. A., "Propagation of Electromagnetic Waves through a Turbulent Atmosphere", Rep. Prog. Phys., pp. 39-112, 1992.

Kravtsov, Y. A., "New Effects in Wave Propagation and Scattering in Random Media (a mini review)", Appl. Opt., 32(15), pp. 2681-2691, 1993.

Lee, R. W. and Harp, J. C., "Weak Scattering in Random Media, with Applications to Remote Probing", Proc. IEEE, 57(4), pp. 375-406, 1969.

Obukhov, A. M., "Sound and Light Propagation in a Weakly Inhomogeneous Atmosphere", Waves in Random Media, 4, pp. 9-19, 1994.

Prokhorov, A. M., Bunkin, F. V., Gochelashvily, K. S. and Shishov, V. I., "Laser Irradiance Propagation in Turbulent Media", Proc. IEEE, 63(5), pp. 790-811, 1975.

Tatarskii, V. I., Ishimaru, A. and Zavorotny, V. U., eds., "Wave Propagation in Random Media (Scintillation)", SPIE Press, Bellingham, pp. 490, 1993.

Distribution list

INTERNAL DISTRIBUTION

1 – Director General

6 – Document Library

1 – G. Potvin (author)

1 – C/SASO

1 – C/EOW

1 – C/SOp

1 – D. Dion (coauthor)

1 – J. L. Forand (coauthor)

1 – L. Bissonnette

1 – G. Roy

1 – J.-M. Thériault

EXTERNAL DISTRIBUTION

1 – DRDKIM

1 – DRDKIM (unbound copy)

1 – L. Gardenal

NuRun Inc.
1260 Boulevard Lebourgneuf, Bureau 250
Québec (Québec) Canada G2K 2G2

1 – P. Lahaie

Aerex Avionique Inc.
36, du Ruisseau, local 102
Breakeyville (Québec)
G0S 1E2 Canada

2 – A. Kohnle

Research Institute for Optronics and Pattern Recognition
(FGAN-FOM)
Gutleuthausstrasse 1
76275 Ettlingen, Germany

1 – P. Adedze

Defence Evaluation and Research Agency (DERA)
Room C-41 West Court, Portsdown West
Portsdown Hill Road
Fareham, Hants. PO17 6AD, England

1 – H. Vogel

Danish Defence Research Establishment
Ryvangs Allé 1,
P.O. Box No. 2715
DK-2100 Copenhagen, Denmark

1 – E. Stark

Norwegian Defence Research Establishment
P.O. Box 25

N-2027 Kjeller, Norway

1 – S. Doss-Hammel, D858

Atmospheric Propagation Branch
SPAWAR Systems Center
San-Diego, CA 92152-7385

2 – Y. Hurtaud

CELAR
Division GEOS
BP 7419
35 174 Bruz CEDEX
France

1 – K. L. Davidson, Code MR/Ds

Meteorology Department
Naval Postgraduate School
589 Dyer Road RM254
Monterey, CA 93493-5114

1 – P. A. Frederickson

Meteorology Department
Naval Postgraduate School
589 Dyer Road
Monterey, CA 93493-5114

1 – Pat D. C. Barnhouse

DSTM3
Defence R&D Canada
National Defence Headquarters
Ottawa, Ontario K1A 0K2

1 – G. J. Kunz

Physics and Electronics Laboratory TNO
P. O. Box 96864
2509 JG The Hague, The Netherlands

1 – A. N. de Jong

Physics and Electronics Laboratory TNO
P. O. Box 96864
2509 JG The Hague, The Netherlands

1 – CDR. Andrea Cini

MARITELERADAR
Viale Italia 72
57100 Livorno, Italy

1 – Tenente di Vascello Marco Licheri

MARIPERMAN
Viale San Bartolomeo
19100 La Spezia, Italy